Review and benchmark study on the analysis of low-velocity impact on composite laminates

Raffael Bogenfeld[*], Janko Kreikemeier, Tobias Wille

German Aerospace Center, Institute for Composite Materials and Adaptive Systems, Lilienthalplatz 7, Braunschweig 38108, Germany

ARTICLE INFO

ABSTRACT

For the analysis of low-velocity impact damage, many analytical and numerical models were developed by various authors. These models range from simple approaches with a single degree of freedom up to finite element models on micro-scale. The prediction of delamination, fiber failure, and inter-fiber damage, as well as a physically sound kinematic behavior, are usually the objectives of these simulations. However, achieving satisfactory results requires massive computation and modeling efforts. In the present paper, we review the capability to capture impact damage on the coupon and the structural level. For this purpose, a large compendium of analytical and numerical analysis methods from various authors is considered. Based on existing works, six representative modeling approaches of different abstraction scales are derived and considered on a qualitative and quantitative benchmark study. We analyze all models regarding their advantages and deficiencies. With two experimental coupon impacts, all approaches are tested on their predictive capabilities on the coupon level. The applicability of these methods on the structural level is evaluated according to the benchmark results. Modeling approaches included in the benchmark range from high-fidelity models on meso-scale, macro-scale shell models, and analytical estimations. The focus is put on stacked layer models with solid or shell elements and various cohesive zone approaches.

With this paper, we also present guidelines for impact analysis strategies on the structural level. These guidelines aim for a good balance between accuracy and computation effort and involve various simplifications of impact scenarios. In this regard, the range of low-velocity has to be monitored. The energy distribution over the eigenmodes of the impact system suitably indicates the limit of low-velocity impact.

1. Introduction

Composite structures are likely to be exposed to impact loads during their service life. Bird strike, hail or tool-drop are typical examples of an impact on an aircraft structure. Usually, impact scenarios are distinguished between Low-Velocity Impact (LVI), High-Velocity Impact (HVI) and ballistic impact. Among these, LVI is of particular importance for the structural lifetime. LVI causes damage inside the material, consisting mainly of delamination [1,2]. Such damage is classified as a Barely Visible Impact Damage (BVID). If no other visible damage-modes occur simultaneously the damage will possibly remain undetected. Even though a significant strength reduction is possible [3], the structure still has to stay capable of bearing the design loads. Sufficient residual strength needs to be ensured for the entire structural lifetime. This problem is often approached by a massive qualification effort with tests on structures and coupons. Besides, conservative knock-down factors increase the designed thickness of structures. In

---

consequence, the significant advantage of a fiber reinforced material — a lightweight design — nearly disappears. Thus, derivation of design improvements by the aid of numerical analysis becomes attractive.

Impact analysis on composite structures has already been a topic of research since the early nineties [4]. Many models that vary in abstraction scale and applied methods were proposed for the last ten years. Recent studies show that it is possible to obtain excellent simulation results through meso-scale finite element models. However, the simulation of impact is still challenging from the numerical point of view. Achieving a sufficient accuracy in a reasonable computation time remains a challenge. For coupon simulations with state-of-the-art models, computation times of one day or more are reported [3,5]. LVI is for one reason mainly critical here: a high impactor-mass m_i results in long contact time — this time needs to be captured by a transient simulation. The computation time increases approximately linearly with the impact duration and is consequently proportional to $\sqrt{m_i}$.

Existing reviews on impact simulation rather focus on details of a selected modeling approach, such as the variation of failure conditions or damage model. With the present work, the authors intend to compare methods in a more general way. A juxtaposition of models on different abstraction scales shall provide the groundwork for weighing up the analysis effort and the result quality of an impact analysis.

For that purpose, we introduce the methods available in the literature and explain the corresponding modeling techniques and fundamental equations briefly. On the basis of the available methods, a choice of six specific methods is made. These shall cover a wide range of abstraction scales and analysis efforts. So, we chose two analytical and four finite element approaches which are all differently costly concerning the model preparation and the result computation.

All models are based on existing publications. Partially, modifications or recombinations were required to ensure their comparability. An evaluation of the methods is conducted through analyzing the predictive capabilities, the modeling effort, and the computational expenses. In the actual benchmark, a direct comparison with the help of two test examples is presented. This comparison relies on experimental data and allows to evaluate the models' performance. Based on the benchmark results, guidelines for impact analysis on the structural level are derived. Several suggested simplifications and idealizations of impact scenarios shall improve the efficiency of impact analysis on the structural level.

2. Review of developments in impact analysis

2.1. Steps of development

The development of impact analysis methods went from simple analytical models to high-fidelity finite element approaches. The overview in Fig. 1 shows the range of methods considered in this review. Each increase of predictive capabilities means a simultaneous increase of the analysis effort. The major aim of impact analysis is the prediction of damage. Already analytical or empirical expressions can provide information about the damage onset and its quantitative dimensions. Numerical models can predict the damage type and shape, depending on the modeling strategy with a different degree of detail.

Early analytical methods treat an impact system as a multi-body system in which springs connect one or more masses. Abrate published the first of such spring-mass models in 1991 [4], and later by Christoforou [6] and others followed. These models capture an elastic impact response, taking into account the plate deformation of the structure and the local surface indentation. Based on a spring-mass model, Christoforou even developed a semi-analytical approach for analyzing impact by dimensionless constants, the so-called loss factor theory [7]. It allows achieving kinematic similarity of size-scaled impact scenarios. These analytical methods permit an estimation of impact duration, maximum contact force, and impactor displacement. Furthermore, Olsson developed an advanced spring-mass model [8,9] that captures damage by a spring in series with the bending deformation. Singh and Mahajan [10] recently enhanced this idea through damage consideration in each deformation mode.

The next higher abstraction level is a plate model. This approach comprises more natural frequencies of the impact system.
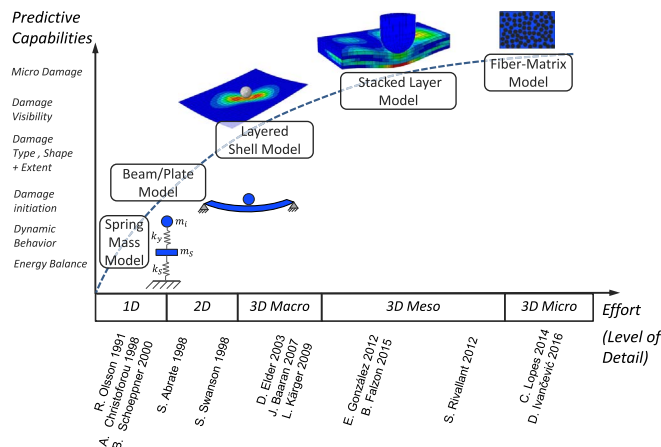

Fig. 1. Overview of impact analysis methods.

Dobyns' development on the dynamics of orthotropic plates [11] forms the basis of those approaches. Building on that, Olsson derived in 1992 the first impact model [12], based on Kirchhoff's plate equation. Besides, Swanson proposed an improved plate approach in 2005 [13] that is also valid for composite laminates [13]. Such plate models capture the undamaged dynamic behavior with higher accuracy than spring-mass approximations. The inclusion of material-specific nonlinearities, as proposed by Najafi in 2016 [14], even extends this capability.

Both spring-mass and plate models can be combined with an empirical or analytical prediction of Damage Threshold Loads (DTL). Analytical estimations of the damage initiation and extent build on such DTL. For instance Olsson, Schoeppner and Abrate have proposed respective methods [8,9,15]. DTL are usually derived using fracture mechanics, to predict the contact force that makes a delamination grow. To predict the damage extent, Jackson and Poe [16] proposed a force-based approach that calculates the largest delamination diameter.

Beyond the possibilities of analytical description, impact analysis can be conducted by the finite element method in many variations. These variations are categorized in macro-, meso- and micro-models, depending on the laminate's abstraction scale of the finite elements. Layered-shell approaches belong to the macro-scale. As proposed by Elder et al. in 2003 [17], such models capture the kinematics of impact like a plate model. But they permit the evaluation of failure conditions on the ply-level and the corresponding stiffness degradation. The model by Elder used explicit simulations in LS-DYNA implementation, Baaran [18,19] and Kärger [20,21] even developed a stand-alone-tool for impact analysis (CODAC[1]). By implicit time integration, combined FE analysis, and analytical equations an efficient impact analysis was achieved.

An upgraded macro-scale model that even included a stacking of sublaminates was published by Johnson et al. in 2001 [22]. This stacking permits to use an interface model between the plies. Johnson applied an interface model from Allix and Ladeveze [23] to capture delamination damage. This method still provides the basis for state-of-the-art meso-scale models. Considering the limited computation power compared to today's possibilities, the results reported by Johnson are of reasonable quality.

The increase of computational power permitted to apply Johnson's idea on a higher degree of detail: Meso-scale FE models capture the laminate by modeling each ply with at least one layer of elements. The majority of recent publications uses such a modeling approach. The plies are equipped with a damage-model based on continuum damage mechanics (CDM) and the cohesive zone method (CZM) according to Allix [23] is used at the interface. There is a vast variety of published meso-scale methods — the interface model, the ply model, element types and meshing approaches are essential characteristics in which recent models differ. As a meso-scale model can work with any homogenized failure condition [24,25], the choice of this condition is also an important parameter.

In 2001, also Borg et al. published a cohesive element delamination model for composite laminates [26]. Based on this model, the research group presented a complete meso-scale model for impact analysis in 2004 [27]. In this model, an approach for determining the propagation direction of delamination was included. Published by Loikkanen el al., another meso-scale model followed in 2008 [28]. They applied the cohesive surface method in their impact analysis model.

In both these works of Loikkanen and Borg, good delamination predictions are reported. Borg additionally identified the necessity of improved ply-damage-models. A correspondingly improved model was presented by Bouvet in 2010 [29] and by Gama in 2011 [30]. Later, several adapted configurations were developed, for example by Shi in 2014 [31], Gonzalez in 2012 [5] and Tan in 2015 [3]. Recent publications mainly provide incremental improvements. Better failure conditions [32], inclusion of nonlinearities and the permanent deformation [3,33-35] or the damage evolution [3,36] are proposed. Panettieri also identified additional relevant influence factors like the vibration behavior of the impactor [37].

Good results can be achieved with these methods, even though the computation effort is high and numerical difficulties have been reported. Recent improvements possibly provide a better solution accuracy, but rather increase the computational effort than reducing it. Usually, user-defined material models are necessary for the CDM damage-models. Especially if permanent indentation or nonlinear shear behavior shall be included, onboard materials of commercial FE codes do not provide the required features. Gama implemented a suitable material model for LS-Dyna and published it under the name Mat162 [38].

While usual meso-scale approaches capture intra-ply damage through continuum damage mechanics, Bouvet and Rivallant developed an alternative solution [29,39]. The mesh aligns with the fiber direction, and fiber-parallel cohesive zones are put inside each ply. In contrast to continuum damage mechanics, cracks are captured as real singularities in the ply. The corresponding failure mode is called ply-splitting [29] and a type of inter-fiber failure. The simulation results of Bouvet show excellent agreement with experimental results on different laminates of unidirectional plies.

Furthermore, other variants to build a meso-scale model without CDM were tried: The extended finite element method (XFEM) XFEM was considered to be suitable for lamina damage by Nian [40] and Chen [41]. But Chen also mentioned difficulties with explicit time integration and the required computation effort. Other advanced methods like phase field modeling [42] or discrete elements [41] do still not provide the required maturity for application on laminated composites.

On the next level of detail, the prediction of inter-fiber fracture is conducted by a micromechanical model. Such a model needs to be coupled with a reference volume element (RVE) in a multiscale approach. The damage onset and the matrix damage are predicted on a micro-scale. Especially for multiaxial loading, such a prediction is superior to homogenized models. Micromechanical failure criteria like Huang [43] or energy based matrix failure conditions [44,45] can be used. Lopes et al published the first impact model on this abstraction scale in 2014 [46], in 2016 Ivančević and Smojver [47] proposed another approach.

---

[1] Composite Damage Tolerance Analysis Code, www.dlr.de/FA.

2.2. Existing reviews

Many researchers already have conducted reviews about impact analysis methods. The compendium ' Impact on Composite Structures' by Abrate [48] represents a review of the entire spectrum of analytical methods. The capabilities and the deficiencies of various spring-mass and plate models are analyzed and evaluated in this work. The first broadly-based review was conducted by Elder et al. in 2004 [49]. Linear elastic fracture mechanics, macro-scale shell-models, and the damage threshold loads were tested. Among these, damage threshold evaluation lead to surprisingly good results. But the test cases were still far from possible impact use cases. For efficient aircraft design application, a need for further development and improved accuracy was determined.

Also about recent high-fidelity models, reviews have been published. A comparison of the predictive capabilities with different failure criteria was conducted by Liu et al. [32]. Their model is based on stacked-solid approach with cohesive elements. According to their results, the Puck criterion leads to the most reliable results. Force history, energy dissipation, and damage initiation forces were plausibly predicted. Other criteria also lead to proper results. In consequence, it is appropriate to trade off between accuracy and computation effort for particular applications.

In 2015, Lopes et al. conducted another benchmark about impact simulation methods [34]. Four different meso-scale modeling strategies with varying mesh structures and cohesive zone models were presented and compared. Aligned meshing improved the prediction of the intralaminar failure and the delamination. Cohesive surfaces permitted to include the friction behavior of two delaminated plies and also lead to improvements in the overall results.

In addition to that, Jousset published a comparison of two different possibilities to employ a constitutive law in a cohesive zone [50]. A standard bi-linear traction separation law was compared to a pressure dependent elasto-plastic damage-model. An elastoplastic model showed a better behavior if the interface material showed significant plastic yield. May's evaluation of cohesive laws [51] included strain rate effects. He provided an overview of the required enhancements and identified strain rate effects as crucial only beyond LVI and quasistatic events. Abisset et al. proved in their work the equivalence of damage morphology between quasi-static indentation and LVI [52]. On the numerical side, the influence of cohesive parameters on the impact response was analyzed by Panettieri et al. [53].

The state-of-the-art modeling approach with a meso-scale model is also used beyond the analysis of LVI [3,32,34,54]. Corresponding models for high-velocity impact were proposed by Pernas-Sanchez et al. [55] or by Heimbs et al. [56]. A comparable approach is also applied for crushing analysis [57] and for general damage modeling in composite structures [58].

2.3. Prediction of damage visibility

In addition to the damage itself, the damage visibility is of significant interest for the numerical prediction. The visibility determines whether a damage will be discovered and repaired. In aircraft application commonly a limit value of permanent indentation at the impact spot is applied to define the visibility limit. Additionally also the fiber crack length on the impact side can be taken into account to assess the visibility. The fiber crack length is predicted by nearly all finite element models accomplishing damage analysis. In contrast to that, additional implementations are necessary to capture the permanent indentation model.

The physical causes of permanent indentation are resin plasticity and the impeded crack closure in the unloading phase [59]. When the crack closes, resin debris can prevent a crack from fully closing. This phenomenon affects both tensile and shear cracks. There are several possibilities reported in the literature to capture it.

The most simple prediction is an empirical description by an analytical formula [48]. Using the contact law of Hertz [60] and a damage threshold permits to compute a value for the permanent surface indentation. The evaluation of such a formula is possible within the postprocessing of most impact analysis methods. For example, Li et al. [61] proposed a corresponding method: based on a finite element model the permanent indentation is captured by an analytical law relying on the Hertzian contact.

Capturing the permanent indentation in a finite element model requires an adaption of the constitutive law. An appropriate model of the unloading phase is essential. The stress has to reach zero before the strain reaches its zero-point. A simple bilinear degradation law does not serve this purpose as the unloading always goes along a secant to the origin. In 2011, Falzon and Apruzzese proposed a method to capture the permanent deformation based on the non-linear shear behavior [58,62]. This method was also applied in the advanced impact simulation model of Tan and Falzon [3]. Fanteria et al. [63] confirmed that the permanent indentation predicted by that method is qualitatively analogous to the indentation in experiments. In a sensitivity analysis, they pointed out that an accurate knowledge about the non-linear shear behavior is significant for quantitative prediction of the indentation values.

Another approach was developed by Bouvet et al. [59]. This approach is based on the previously mentioned ply-splitting model with intra-ply cohesive zones. The constitutive law of the cohesive elements capturing matrix damage is adapted. After tensile or shear damage occurred, a stress of zero is reached before the strain reaches zero. The element responds with compression stress if the strain becomes smaller than this predefined value. This law shall directly describe the effect of resin debris blocking the crack.

Lopes et al. suggest another alternative that works with a cohesive surface model [34]. They used the static friction of opposing crack planes prevents the delamination from closing. That way, also a permanent deformation is described.

Apart from the visibility, the permanent indentation has also a significant influence on the energy absorption as Caprino et al. showed in their study [64] and confirmed by Fanteria et al. [63]. After the impact, residual stresses remain in the laminate. This elastic energy also contributes to the total energy absorption. Accordingly, models without a permanent indentation model underestimate this value. Although the prediction of permanent indentation is not part of the benchmark in this study, it is important to mention that its prediction is also a crucial part of LVI analysis as it determines the visibility.

2.4. Impact analysis on the structural level

Sufficiently accurate modeling strategies are available, the current challenge is the application of impact analysis on the structural level. While the predictive capabilities seem satisfactory, the corresponding computation effort is already very high for small coupon specimens. For coupon simulations of CAI impacts, Tan reports a computation time of 19 h on 32 CPUs [3], Lopes even 48 h on 40 CPUs, as a very fine mesh was applied. These numbers show that a blunt transfer of the same method to structural level would result in inefficiently high computation effort. For some methods, also the modeling effort can severely increase.

An excellent example for a structural application of a high-fidelity impact analysis was published by Schwab and Pettermann in 2016 [65]. The definition of a damage-prone area permits to work with differently meshed zones. Riccio proposes in several publications a comparable approach [66,67]. He also applies a local analysis approach with a damage-prone area and uses it already on the coupon level in order to reduce the computational costs. Both, Riccio and Schwab achieved good results with this local impact damage analysis. Also, Riccio presented the application of a meso-scale model on a substructural level [68]. Johnson works directly with a cut-out section of the actual structure [69]. Low-fidelity methods with a layered-shell mesh can directly be applied on the structural level, as the number of DoF is significantly lower [20].

3. Applied damage prediction methods

While the previous section was a summary about impact analysis models, this section includes a brief description of the essential methods for crack and damage prediction within these models. The modeling approaches in the following benchmark are based on the features described in this section.

3.1. Delamination threshold forces

The determination of threshold forces for the onset of delamination and fiber cracking is crucial to assess the impact damage through analytical models. The associated formulas are based on analytical relations between the laminate characteristics and an out-of-plane loading. A combination with any impact model that predicts the contact force history is possible.

An analytical formula for a delamination threshold F_d that was defined by Olsson [70] is written in Eq. (1). In this equation, the integer variable n_{del} represents the number of delaminating interfaces. G_{IIc} is the critical energy release rate in mode II, the parameter D^* represents the effective bending stiffness of the laminate according to Eq. (2). In an earlier work, Olsson derived this parameter from the bending stiffness entries of the classical laminate theory [12]. C is an analytical factor which is one for the quasistatic solution of LVI. Taking dynamic effects into account, Olsson analytically derived a value of $C \approx 1.213$ for intermediate-velocity impacts [70].

$$F_d = C\pi\sqrt{\frac{32G_{IIc}D^*}{n_{del} + 2}}$$

(1)

$$D^* \approx \sqrt{D_{11}D_{22}\frac{1 + \frac{(D_{12} + 2D_{66})}{\sqrt{D_{11}D_{22}}}}{2}}.$$

(2)

Olsson even derived an analytical formula for the approximation of the accumulated delamination area of all interfaces $A_{d\text{-}total}$ (Eq. (3)) [9]. Assuming that the delamination growth is driven by mode II, the energy dissipation W_{loss} is related to G_{IIc}. In this equation, F_0 and w_0 represent the impactor force and displacement after the completed delamination growth, F_d and w_d are the corresponding values at the delamination onset.

$$A_{d-total} = \frac{W_{loss}}{G_{IIc}} = \frac{(F_d + F_0)(w_d - w_0)\left(1 - \frac{7\pi^2}{216}\right)}{4G_{IIc}}.$$

(3)

Jackson and Poe proposed a second possibility to estimate the delamination size analytically. Their formula in Eq. (4) does not build on the energy dissipation W_{loss} but on the interlaminar shear strength X_{shear} and the ply thickness t. That way, it correlates the maximum contact force F_{max} directly to a delamination diameter. Under the assumption of a circular delamination shape, the maximum delamination diameter can be converted to the corresponding area A_{dela}.

$$A_{dela} = \frac{1}{\pi}\left(\frac{F_{max}}{2tX_{shear}}\right)^2.$$

(4)

These analytical estimations assume identical delaminations in all delaminating interfaces. Consequently, the projected delamination area would be equal to the delamination area in each single interface. This idealization makes a comparison of the analytical value with experimental results difficult. Firstly, the distribution of delamination area in an impact experiment is not equal among all interfaces. Secondly, the delaminations are not stacked congruently. Both effects increase the real projected delamination area, though the accumulated area could remain constant. With the analytical approaches, underestimation is inevitable. Instead, the accumulated delamination area over all interfaces would be a better comparative value for these methods.

3.2. Cohesive zone method(CZM)

The key feature of an FE meso-scale approach is the interface model between the plies. At this interface, a cohesive zone method is employed to capture delamination damage. In contrast to the VCCT method, no initial crack is required for the cohesive zone approach. Therefore a CZM is preferred for impact analysis. It is a fracture-mechanical method which describes the initiation and the propagation of a crack in a predefined interface. The basic ideas for the CZM were developed by Dugdale [71] and Barenblatt [72]. Allix and Ladeveze [23] were the first to present a corresponding interface model to capture delamination damage.

In the initial state of the interface, the cohesive zone connects both interface partners elastically. This connection concerns three deformation modes that all lead to a separation of the partners: the deformation mode in normal direction and two out-of-plane-shear deformation modes. In each mode, a stiffness component K_{ij} and a relative displacement δ_{ij} permit the calculation of a traction t_{ij} through Hooke's law in Eq. (5). The stiffness components K_{ij} have the unit [N/mm^3] and stand for stress per separation. The tractions describe the state of stress in the interface zone, and a damage initiation condition can be evaluated. When damage initiates, a traction separation law describes the softening behavior of the interface.

$$\mathbf{t} = \begin{pmatrix} t_{nn} \\ t_{nl} \\ t_{nt} \end{pmatrix} = \begin{bmatrix} K_{nn} & & \\ & K_{nl} & \\ & & K_{nt} \end{bmatrix} \begin{pmatrix} \delta_{nn} \\ \delta_{nl} \\ \delta_{nt} \end{pmatrix}.$$

(5)

A cohesive zone can be employed in the form of cohesive elements and the form of cohesive surfaces. Eq. (5) represents the formulation for cohesive surfaces. Cohesive elements work with a constitutive thickness value T_0 to compute strain values from the separations. The stiffness values of cohesive elements respectively require a multiplication with this thickness: $K_i T_0 = E_i$. In both cases, the stiffness of the cohesive zone is rather numerical than a physical parameter. In order to maintain physical soundness, the stiffness has to be high enough not to influence the global laminate stiffness significantly. For the derivation of a quantitative value for K, Turon [73] suggests that the ratio of the cohesive stiffness K and the ply stiffness $\frac{E_{33}}{T_{ply}}$ shall be at least 50. After the failure condition indicates damage initiation, the energy release rate G_i becomes the driving parameter. It determines the constitutive law of the interface-softening.

Although the CZM is suitable for delamination prediction in impact analysis, it entails several difficulties. These concern the parameters of the cohesive zone, the additional mass and compliance [73] in the laminate as well as the additional computational effort. For numerical reasons, also a modification of the cohesive zone's strengths (maximum tractions) can be required. Even though physically incorrect, this method is well-suited to permit larger element lengths in the cohesive zone. Turon et al. [73], later also Harper and Hallett [74], analyzed this method in detail, and Panettieri et al. examined the application for impact simulation [75].

Turon proposed Eq. (6) to estimate the required minimal element length l_e for a cohesive zone in a ply interface. In this equation N_e stands for the number of elements in the cohesive zone. According to Turon at least three should be chosen, here. E is the elastic modulus of the corresponding deformation mode, and $\sigma_{\max}$ the failure stress for damage initiation.

$$l_e = \frac{9\pi E G_c}{\sigma_{\max}^2 \, 32 N_e}.$$

(6)

3.3. Continuum damage mechanics(CDM)

Many impact analysis methods make use of a CDM approach to capture the intra-ply failure modes. The CDM concept was developed by Chaboche and Lemaître in 1980 [76]. Its basic principle is the homogenization of a crack. The effective stress σ results from the nominal stress $\hat{\sigma}$ by multiplication with a factor $(1 - d)$ in Eq. (7). This factor represents the ratio of the remaining load carrying cross-section and the initial cross-section. The parameter d describes the degradation status.

$$\sigma = (1 - d)\hat{\sigma} = (1 - d)E\varepsilon.$$

(7)

Matzenmiller expanded this method for two-dimensional states of stress and orthotropic materials [77]. Six degradation variables d_i are necessary to describe the degradation status of a material point under a three-dimensional state of stress. One for each normal and shear deformation mode. This number increases to nine if compression and tension are considered as separate failure modes. Depending on the normal stress, only one of two damage variables for each normal mode becomes active according to Eq. (8). This is achieved through the Macaulay brackets in the fraction $\frac{\langle \sigma_{nn} \rangle}{\sigma_{nn}}$. It returns zero for a negative and one for a positive σ_{nn} [78].

The quantitative value of the damage variables are usually obtained through a bilinear damage evolution law like in Eq. (9) and illustrated in Fig. 2. The strain of damage initiation ε_i results from the failure condition. The critical energy release rate G_c of the corresponding damage mode defines the integral value of the bilinear curve. As a result, the ultimate failure strain ε_u is determined.

$$d_i = d_{i+} \frac{\langle \sigma_{nn} \rangle}{\sigma_{nn}} + d_{i-} \frac{\langle -\sigma_{nn} \rangle}{\sigma_{nn}}$$

(8)

$$d(\varepsilon) = \frac{\varepsilon_u}{\varepsilon_u - \varepsilon_i} \left(1 - \frac{\varepsilon_i}{\varepsilon} \right).$$

(9)

A combination of CDM with any homogenized failure criterion [25] is possible. However, it requires an analysis trick. Damage evolution is not independent in each strain component. It occurs a fracture plane of the corresponding damage-mode [36]. For
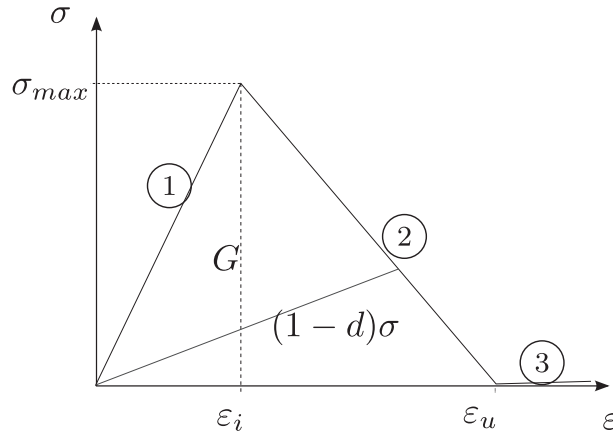
Fig. 2. Bilinear constitutive law.

degradation in a fracture plane, a scalar equivalent strain value has to be obtained. This is accomplished through the three strain components in the fracture plane. Most authors work with a root sum squares method like in Eq. (10). The computation of ε_u additionally requires an equivalent stress as reported in Eq. (11). The sketch in Fig. 3 depicts the fracture plane coordinates *n, l, t*. Fracture plane stresses and strain are defined in these coordinates, where *nn* stand for the normal component while *nl* and *nt* represent the shear components.

$$\varepsilon_i = \sqrt{\langle \varepsilon_{nn} \rangle^2 + \varepsilon_{nl}^2 + \varepsilon_{nt}^2} \tag{10}$$

$$\sigma_i = \sqrt{\langle \sigma_{nn} \rangle^2 + \sigma_{nl}^2 + \sigma_{nt}^2}. \tag{11}$$

Another important issue is the scaling of ε_u by the characteristic element length of the damage-mode. This scaling becomes necessary because the strain energy in the element depends on the element volume V_e, while the energy absorption by a crack G_c depends on the corresponding crack surface A_i. Accordingly, $\frac{V_e}{A_i}$ defines the required length parameter l_{ic}.

$$\varepsilon_u = \frac{2G_c}{l_{ic}\sigma_i} \tag{12}$$

Eq. (12) results in a limitation of the maximum allowed element length for each damage mode because the condition $\varepsilon_i < \varepsilon_u$ shall always be fulfilled. This leads to Eq. (13) limiting the element length l_e.

$$l_{e-\max} = \frac{2EG_c}{\sigma_i^2}. \tag{13}$$

Suitable CDM material models are available in most commercial FE codes. For example in Abaqus, the Hashin criterion [79] and an appropriate damage evolution are provided for shell elements. For LS-Dyna, the material model MAT162 offers the corresponding

$$\varepsilon_i = \sqrt{\langle \varepsilon_{nn} \rangle^2 + \varepsilon_{nl}^2 + \varepsilon_{nt}^2}$$

$$\sigma_i = \sqrt{\langle \sigma_{nn} \rangle^2 + \sigma_{nl}^2 + \sigma_{nt}^2}$$
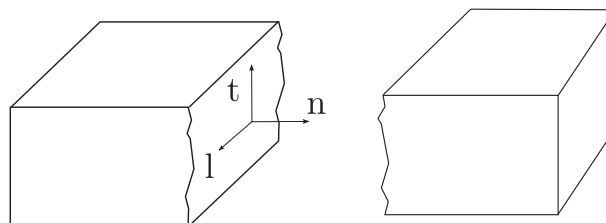

Fig. 3. Sketch of the coordinates fracture plane and the coordinate systems.

Table 1
Overview of six modeling approaches to be benchmarked.

	Spring mass	Ortho. plate	Layered shell	Stacked-shell	Stacked-solid	Splitting
Abstraction scale	Global impact system	Macro	Macro	Macro-meso	Meso	Meso
Ply elements	Homogenized in a spring	Analytic plate	S4R[a]	S4R[a]	C3D8R[b]	C3D8R[b] + COH3D8[c]
Interface	–	–	Integration point	COH3D8[c]	Cohesive surfaces	COH3D8[c]
Analysis environment	Scilab	Scilab	Abaqus standard	Abaqus explicit	Abaqus explicit	Abaqus explicit
Delamination	Threshold force	Threshold force	Quad strain	Quad strain	Quad strain	Quad strain
Fiber failure	–	–	Max strain	Max strain	Max strain	Max strain
Inter-fiber Failure	–	–	Hashin	Hashin	Quad strain	Quad strain (cohesive elements)
Damage Evolution	–	Secant stiffness limit	Bilinear	Bilinear	Bilinear	Bilinear
Closest literature Models	Abrate 1991 [4]	[11,12]	Baaran 2003 [18], Karger 2008 [20]	[41]	Liu 2016 [32]	Hongkarnjanakul 2013 [80]

[a] Linear shell elements with reduced integration.
[b] Linear solid elements with reduced integration.
[c] Cohesive elements.

features. Anyway, an implementation in a user subroutine is commonly used. The gain of flexibility to implement various failure conditions, damage evolution equations or non-linearity models is of value for improvement of the result-quality. For application in the present work, a VUMAT implementation for Abaqus explicit was accomplished. A CDM approach was employed according to the equations in this section. The criterion in Eq. (14) was used as the failure condition. The parameter α was set to one for inter-fiber failure (Quad strain criterion) and to zero for fiber failure (max strain criterion). In consequence, six separate damage-modes have to be considered — compression and tension in each direction of the material coordinate system.

$$F_n = \sqrt{\left(\frac{\varepsilon_{nn} E_{nn}}{X_{nn}}\right)^2 + \alpha \left(\frac{\varepsilon_{nl} E_{nl}}{X_{nl}}\right)^2 + \alpha \left(\frac{\varepsilon_{nt} E_{nt}}{X_{nt}}\right)^2}.$$

(14)

4. Implemented impact models for comparison

In this section, we introduce the six modeling approaches to be tested in the benchmark. These are composed of two analytical and four numerical methods. The descriptions include a summary of the models' key features concerning the laminate description and the corresponding damage model. This section does not describe the modeling of the actual impact scenario with its boundary conditions and impactor. These features will later be explained in Section 5.1, because they are not part of the method itself but rather depending on the specific application scenario.

Table 1 provides an overview of the key characteristics of all approaches. Also, the most important source of literature for each model is listed there. However, the applied models in this work are not equal to the literature models. The conducted simplifications and modifications were necessary to ensure the comparability of the different models. In some cases, these changes can be responsible for discrepancies of the results.

4.1. Spring mass model

The first model for the benchmark is the most simple way to analyze an impact event. Therefore, a spring-mass model with a single degree of freedom is set up as shown in Fig. 4. A point mass m_1 and a linear spring k_1 represent the impact system. This is an
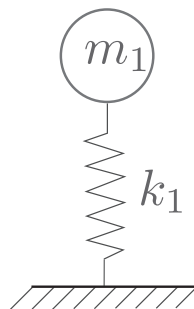

Fig. 4. Spring mass models of an impact system.

idealization in several ways: vibration modes of higher-order and effects of non-linearity are fully neglected. The bending, the shear deformation, the membrane deformation and the surface indentation [60] are all summarized and linearized through a scalar stiffness variable.

The parameter determination is also simple. The mass m_1 consists of the impactor mass m_i and the modal mass belonging to the lowest structural eigenmode participating in the impact. While the first is quite high for low-velocity impact, the latter is quite small and $m_i \approx m_1$ becomes a reasonable approximation. An estimation of the stiffness k_1 can be done using experimental impact data, a finite element analysis or for simple geometries with an analytical approximation.

This linear model with constant parameters can approximate the impact duration $t_i = \sqrt{\frac{m1}{k1}}\,\pi$, the maximum impactor displacement $x_{\max} = \sqrt{\frac{2E_i}{k_1}}$ and the maximum contact force of $F_{\max} = \sqrt{2W_i k_1}$. If k_1 was determined for the undamaged system, force and indentation can be regarded as theoretical maxima for a given impact scenario.

Damage estimations are conducted with the presented analytical methods from Section 3.1. The damage threshold formula in Eq. (2) from Olsson is evaluated. The delamination area is estimated with Jackson and Poe's method given in Eq. (4).

4.2. Plate model

With a plate model, a second analytical method is included in this benchmark. The basic principle of this model derives from Dobyns' idea [11] for capturing the dynamic behavior of orthotropic plates. Simply supported boundary conditions are applied and only bending deformation is taken into account in the present study. For that case, the indentation w of the composite plate is calculated based on the differential Eq. (15). The indices x and y represent the respective derivatives of w. The coefficients D_{ii} are the plate stiffness constants from the classical laminate theory.

$$D_{11}\, w_{,xxxx} + 2\,(D_{12} + 2\,D_{66})\, w_{,xxyy} + D_{22}\, w_{,yyyy} = f \quad . \tag{15}$$

According to Dobyns' the solution of this equation is approached by a series of sine functions for the indentation w and the load f. To include effects of surface indentation z, this plate theory is combined with the contact model of Hertz [60] in Eq. (16). The impactor displacement x is the sum of w and z.

$$F(z) = k_h\, z^{\frac{3}{2}}. \tag{16}$$

Based on these two equations, an elastic response of the impact system can be obtained. A simple damage model that is based on a damage threshold force extends this plate model. If the contact force exceeds the threshold the surface indentation value z_1 is saved. The following surface indentation $z - z_1$ is seen as irreversible and linear with a reduced stiffness. This value has to be derived from experimental impact data of the impact scenario to be analyzed.

Finally, the equation of motion $F + m_i\ddot{x} = 0$ is set up for the solution of the impactor displacement x numerical time integration is required. This solution procedure was implemented in Scilab[2]. The damage threshold force is obtained by Olsson's method in Eq. (2). For determination of the damage size, the delamination area is estimated with Jackson and Poe's method given in Eq. (4).

4.3. Layered-shell model

The layered-shell model represents the very basic method of impact simulation through the finite element method. A single layer of linear, reduced-integrated shell elements represents the entire specimen layup as the illustration in Fig. 5 shows (S4R with enhanced hourglass control in Abaqus [81]). These shell elements are so-called layered-shells because the laminate is taken into account within the shell element. The shell stiffness is calculated through a laminate theory. For evaluation of stresses and strains in each ply, at least one integration point per ply is necessary. An advanced technique of this model includes the interfaces in addition to the actual plies according to the model sketch in Fig. 5. At least one integration point represents each ply interface that can delaminate. These interface layers have the properties of the matrix material. The evaluation of a delamination criterion becomes possible directly at the interface. Respectively, ply failure is calculated at the plies' integration points, using the built-in Hashin criterion from Abaqus. A bilinear progressive-damage model for intra-ply failure and delamination is applied.

The required mesh density of this method depends only on the desired accuracy of the damage result. Consequently, a layered-shell model needs only a few degrees of freedom and implicit time integration makes sense. In the transient impact analysis, this implicit time integration permits quite large time-increment in comparison with explicit methods.

4.4. Stacked shell model

This model is the first representative of the meso-scale. A stacked shell approach as illustrated in Fig. 6 is the respective most simple variant. Linear, reduced-integrated shell elements with enhanced hourglass control represent each unidirectional layer. Cohesive volume elements with eight nodes (COH3D8 in Abaqus [81]) connect the layers. Tie constraints couple the cohesive layer to each neighbor ply. This coupling is computationally more expensive than shared nodes between both plies but offers more flexibility concerning the mesh in interface and ply. As Abaqus offers an appropriate continuum damage mechanics model for shell elements,

---

[2] www.scilab.org.

Fig. 5. Layered-shell approach without (top) and with interface plies (down).

Fig. 6. Layup model schematics of the stacked shell approach.

this stacked-shell model can be fully realized through onboard-means of Abaqus. The damage model is based on the Hashin failure condition [79] and applies a bilinear degradation law as described in Section 3.3. A detailed description of this damage model can be found in the analysis user's guide of the Abaqus documentation [81]. While the mesh density of the ply mesh still depends only on the desired accuracy of the damage results, the numerical issue makes demands on the mesh density of the cohesive plies. Due to a large number of degrees of freedom, implicit time integration would be inefficient for this approach. Consequently, this and all other meso-scale approaches in the present benchmark are conducted with explicit time integration.

4.5. Stacked-solid model

The stacked-solid model in this benchmark works analogously to a stacked shell model in Section 4.4, but each ply is represented by one layer of brick elements like in the model by Tan [3]. With linear, reduced-integrated brick elements (C3D8R with enhanced hourglass control in Abaqus [81]), it is an extension of the stacked-shells. The solid elements consider out-of-plane stresses and strains entirely. The direct extension of the presented stacked-shell model would be a stacked-solid model with cohesive elements. However, for the stacked-solid model in this benchmark, two more changes are employed.

Firstly, the cohesive elements are replaced by cohesive surfaces as shown in Fig. 7. In contrast to shell elements, solid elements permit the direct application of cohesive surfaces. A direct comparison of cohesive elements and cohesive surfaces is not part of the present paper. A suitable direct comparison of both methods was already established by Lopes [34]. In this reference, better results were reported for cohesive zone surfaces, which is another reason to prefer cohesive surfaces to cohesive elements in this work.

The second difference is the continuum damage mechanics model. For solid elements, there is no suitable model available in Abaqus explicit. Accordingly, a user-defined material model must be applied. For that purpose, the method described in Section 3.3 is applied to capture intra-ply damage by the solid elements.

In contrast to the general description of the CDM method in the Section 3.3, this stacked solid model works with only five damage modes of the quadratic strain criterion. The tensile mode in out-of-plane direction was deactivated, as the respective fracture plane is to the in-plane directions of the laminate. Therefore, the corresponding damage would produce an echo in the ultrasonic d-scan analysis — the damage would be detected as a delamination. The numerical model shall capture the corresponding damage with a single damage variable, which is the damage status of the cohesive zone for this model. Even though this modification relocates damage from the ply to a neighboring interface, the impact solution is hardly affected. Anyhow, for improved accuracy it is recommended to work with all ply-damage modes.

4.6. Ply-splitting model

The ply-splitting model is a very advanced variant of the stacked-solid model. Hongkarnjanakul et al. developed this approach and obtained excellent delamination results with it [80]. For that reason, we consider a model based on Hongkarnjanakul's approach in the present benchmark. In comparison to the previous stacked-solid model, the inter-fiber failure model is changed now. Fiber-parallel cohesive zones are placed within the ply like the illustration in Fig. 8 shows. In contrast to the continuum damage mechanics, the cohesive zone method captures a crack as a singularity. That way, the fiber-parallel splitting of plies is included without homogenization. A precondition for this approach is that the element edges in the ply mesh align with the fiber orientation. In
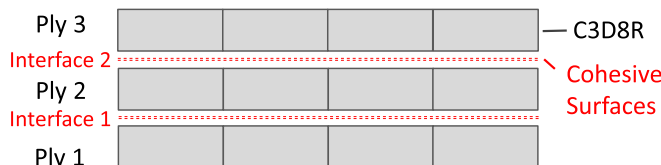
Fig. 7. Schema of the stacked-solid model with cohesive elements (top) and cohesive contact (down).
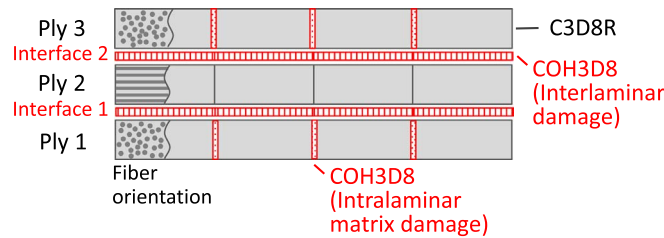
Fig. 8. FE Model.

contrast to the original model by Hongkarnjanakul, in the present study, we did not consider permanent indentation effects and applied a simple bilinear damage law for the inter-ply and intra-ply cohesive zones.

Apart from the intra-ply cohesive zones, this model is similar to the stacked-solid approach in Section 4.5. However, the continuum damage mechanics model is switched off for tensile matrix damage as this failure mode is now captured by the cohesive zones.

5. Benchmark

This section describes the actual benchmark. It begins with the introduction of the experimental test cases. By these test cases, the evaluation of the presented methods from Section 4 follows, comprising three different aspects: the analysis results and the efforts for the computation and the model building.

5.1. Impact test cases

The experimental reference for the benchmark is a simple impact configuration on a flat specimen. Test cases on the coupon level meet the requirements of the impact benchmark because the LVI damage is a local phenomenon [82]. A standardized coupon test setup exists for the compression after impact test in a drop tower. Standards of ASTM, DIN and AITM [83–85] define its configuration almost similarly. A specimen with the in-plane dimensions $150 \times 100 \text{ mm}^2$ and a thickness of 4 mm is impacted on a frame with a $125 \times 75 \text{ mm}^2$ cutout. The impactor shall be hemispherical with a diameter of 16 mm. Despite the small coupon dimensions, all important damage effects can occur. The testing procedure is well known, and there are many published results available for comparison.

The two reference cases to be compared with the simulation results differ in the type of material, the layup, and the impact energy. The first case is taken from literature. Additionally, a second test case was taken from an in-house testing campaign that was conducted by Dienel and Tamer, other researchers from our institute.

- *Test case 1:* 25 J impact on quasi-isotropic T700/M21 layup
  This test case was originally published by Hongkarnjanakul et al. in 2013 [80]. The referenced paper includes a testing campaign with several laminates manufactured from the *T700/M21* material. Among those laminate, the selected test is originally named 'A1'. The layup consists of eight double plies with a thickness of 0.5 mm: $[0_2,45_2,90_2, -45_2]_s$. This stacking leads to quasi-isotropic in-plane properties. Hongkarnjanakul et al. also provide the necessary material data. This test case was already applied for validation by several authors [3,32,86]. So its application in the present study facilitates the comparison of the results with other works. However, as there is no data about experimental scatter available in the original paper, a discussion of the scatter is not possible.

- *Test case 2:* 40 J impact on clustered IMA/M91 layup
  The second case is taken from a testing campaign that Dienel and Tamer conducted and published in 2015 [87]. They used an asymmetrical, clustered layup, consisting of 22 plies: $[45,45,45,0, -45, -45, -45,90, -45,0,45]_s$. The ply-material is an M91 prepreg with the intermediate modulus fiber IM7 and a ply thickness of 0.184 mm. The material data is supplied in the mentioned publication by Dienel. Additionally, there is a data sheet provided by the manufacturer Hexcel [88].
  The availability of several history curves permits an evaluation of the results with the background of experimental scatter. The range of result values is very valuable, as large scatter can be expected for impact damage.
  Due to the clustered characteristics, this layup has only 12 interfaces that can delaminate. For that reason, the delaminations of each interface can reliably be identified in the ultrasonic D-Scan result.

5.1.1. Material parameters and minimal elements length

The required material data for both test cases are provided in Table 2. The data was taken from the publications of Hongkarnjanakul and Dienel, as well as from a data sheet of Hexcel [80,87,88].

With these material parameters, the minimal element length for the FE methods can be derived. The minimal required element length for all four FE models depends on the intra-ply damage parameters and is defined according to the Eq. (13). For cohesive zone methods, the interface model also requires a minimal element length according to the Eq. (6) by Turon.

The minimal lengths values $l_{e\text{-min}}$ for the given set of material parameters are listed in Table 3. The minimum value in each

Table 2
Applied material properties for the benchmark simulations.

		T700/M21	M91/IM7
Density	[kg/m^3]	1600	1570
E_{11t}	[GPa]	130	170
E_{11c}	[GPa]	100	150
E_{22t}	[GPa]	7.7	8.8
E_{22c}	[GPa]	7.7	9.4
E_{33}	[GPa]	7.7	9.0
G_{12}, G_{13}	[GPa]	4.8	5.5
G_{23}	[GPa]	4.8	4.5
ν_{12}, ν_{13}	[–]	0.33	0.228
ν_{23}	[–]	0.48	0.48
X_{11t}	[MPa]	2080	2700
X_{11c}	[MPa]	1100	1590
X_{22t}	[MPa]	60	105
X_{22c}	[MPa]	180	252
X_{33c}	[MPa]	180	252
X_{12}, X_{13}	[MPa]	110	105
X_{23}	[MPa]	65	65
G_{Ic}	$\left[\frac{mJ}{mm^2}\right]$	0.5	0.5
G_{IIc}, G_{IIIc}	$\left[\frac{mJ}{mm^2}\right]$	2.1	2.1
G_{f+}	$\left[\frac{mJ}{mm^2}\right]$	110	106
G_{f-}	$\left[\frac{mJ}{mm^2}\right]$	35	81
G_{m+}	$\left[\frac{mJ}{mm^2}\right]$	0.5	0.3
G_{m-}	$\left[\frac{mJ}{mm^2}\right]$	2.1	0.8
$G_{m-shear}$	$\left[\frac{mJ}{mm^2}\right]$	2.5	2.5
X_{sh}	[MPa]	50	50
X_n	[MPa]	20	20

column defines the minimum element for the corresponding impact model. In this case, this value would be 0.2 mm. However, this value is too small to analyze an impact efficiently. For that reason, a modeling assumption is used for the FE methods in the present study. Other authors also work with much larger elements. The highest mesh density in an impact analysis model was reported by Gonzalez with 0.3 mm [5]. We considered this value as too small for an efficient impact analysis. The 0.2 mm-requirement is driven by the matrix compression failure mode 'G_{m+}'. Thus, a larger element length violates the energy release rate of this mode. We decided that the violation is tolerable for compression failure because the real energy absorption of compression damage is higher than the energy release rate for a single crack. It depends on the crushing of the material after the crack propagation [89] and needs a more advanced constitutive law. In this case, the increased energy absorption is included in the bilinear law. Therefore, 1 mm was chosen for the damage-prone ply elements and cohesive elements.

5.1.2. Model building

Both test cases were conducted by the same CAI standard. Thus, the boundary conditions for both are similar. The CAI test setup, consisting of the support frame, four clamps, and the impactor were modeled as own parts of finite elements as the Fig. 10 shows. Contact definitions between the specimen and the test setup ensure the physically plausible interaction. The applied contacts between the specimen and the test setup are indicated in Fig. 9. The price for this level of detail is an increased number of degrees of freedom

Table 3
List of the minimal element length required by each damage mode.

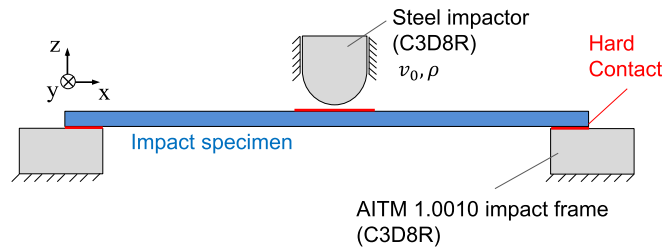|	T700/M21	M91/IM7
Damage mode	$l_{e\text{-}min}$ [mm]	$l_{e\text{-}min}$ [mm]
'G_{Ic}'	1.8	1.2
'G_{IIc}'	1.2	2.1
'G_{f+}'	6.6	4.9
'G_{f-}'	5.8	9.6
'G_{m+}'	2.1	0.5
'G_{m-}'	1.0	0.2

Fig. 9. Schematics of the finite element model with contact definitions indicated in red. (For interpretation of the references to color in this figure legend, the reader is referred to the web version of this article.)

and contact definitions. Each FE method from Section 4 uses this FE test setup and only requires exchanging the laminate model of the specimen.

The analytical models cannot work with contact definitions. Instead, equivalent boundary conditions have to be found. Simple support at the outer edges of the specimen leads to a response that is too soft. Simple support at the edge of the cut-out in the support frame is too stiff. For that reason the mean value between these extreme values was applied: the effective size for the plate model analysis with simply supported boundary conditions was set to 137.5×87.5 mm^2.

5.2. Analysis results

The evaluation of the test results is carried out on the basis of observable damage-modes, history data, and some distinctive values characterizing the entire impact, listed in the following:

- *Delamination damage:* The major failure mode of a Barely Visible Impact Damage (BVID) is delamination [48]. The ultrasonic analysis is applied to detect the delamination inside the specimen. Comparing the ultrasonic results with the simulation, a qualitatively plausible prediction of shape and orientation for each delamination is important. Quantitatively, the projected delamination area over all interfaces is a common reference value. However, the scattering of the projected delamination are is usually large.
- *Fiber cracking:* Without an X-ray analysis, fiber cracks are visible only in the outermost plies. The prediction of their size and orientation is important. In the two experimental test cases, fiber cracks occurred only on the impact side occurred in the top ply. Only this fiber crack will be evaluated in the benchmark.
- *Matrix cracking:* Typically, large inter-fiber cracks appear at the impact backside in the lowermost ply. Straight, sharp cracks arise in the direction of the fiber orientation. They are visible and can be compared to the simulation results.
- *Force-time history:* This history curve is significant because it provides information about the participating frequencies of the impact. Also, their influence on the damage threshold forces can be seen here.
- *Force-displacement history:* In addition to the force-time history, this plot shows the specimen stiffness for each moment of the impact process. In addition, the energy absorption can be deduced from it.
- *Energy dissipation:* As a characteristic value of the impact damage, the total energy dissipation W_{dis} is taken into account. It results from the difference of the impactor's kinetic energy before and after the impact.

5.2.1. Test case 1: 25 J impact on quasi-isotropic laminate

Consisting of eight double layers, this layup has only six possible delamination interfaces. This limited number allows the individual comparison of the delamination in each interface, as presented in Table 4. This overview provides a general impression
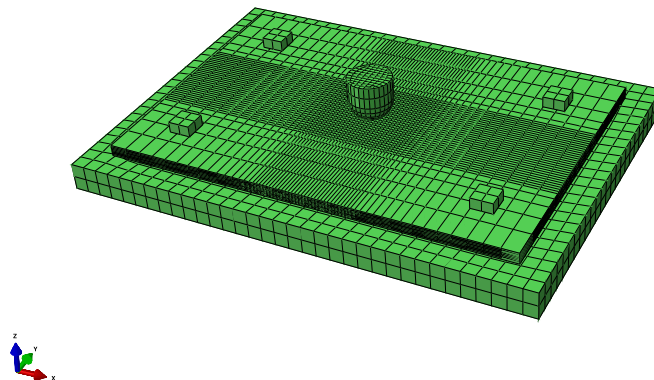

Fig. 10. Assembled finite element model of specimen and impact test rig.

Table 4

Delamination damage of the 25 J impact on the layup A1 reported in Ref. [80]. Interface 1 is the farthest from the impact side.

Inter-face	Springmass + Poe' seq.	Orth. plate + Olsson's eq.	Layered shell	Stacked-shell	Stacked-solid	Splitting	Test result
1							
2							
3							
4							
5							
6							

about the models' capabilities for delamination prediction. On first sight, it is striking that the results of the analytical methods systematically differ from the results of the FE methods which is a result of the simple character of the analytical methods. The damage prediction is limited to a scalar value in the form of the largest diameter. As there is no information about the distribution in thickness direction provided, the same delamination shape is assumed for all interfaces. In contrast to that, all FE models are capable of predicting the pattern of each delaminated interface.

The history curves in Fig. 11 complement the graphical overview. The curves in this figure are separately displayed for the analytical and the FE models because it permits better distinction of the curves. There is nearly no progressive damage behavior in the results of the analytical methods and the layered-shell method. These results suggest the need of a meso-scale approach for an appropriate impact analysis.

For a quantitative comparison, the essential values of the damage and the history data are listed in Table 5. From these results, we conduct a step by step evaluation of each model in the following paragraphs. We point out the advantages and the deficiency of each method and discuss the peculiarities.

The spring-mass model describes the impact force history with a sine curve, based on the linearized stiffness and the impactor mass. The respective estimation of the maximum contact force was expected to be larger than the experimental value because there is no progressive damage law included in this model. This expectation was found to be true, as the predicted contact force is around 2 kN larger than in the experiment. For the same reason, the contact time, as well as the maximum indentation, are underpredicted and the energy dissipation is zero.

The delamination threshold F_d was predicted by Olsson's equation and lead to a solid result close to the experimental value. However, the estimation of the delamination area through Poe's equation is severely too low. This behavior was already expected and explained in Section 3. Only the accumulated delamination area in all interfaces could be a reliable comparative value.

The orthotropic plate model shows an initial response that is similar to the prediction of the spring-mass model. After the damage initiation, a slight degradation of the stiffness can be observed. Consequently, the overestimation of the maximum force is with 1.5 kN smaller than the elastic value. The maximum indentation value d_{max} increased accordingly. Through the progressive damage law, the energy dissipation W_{dis} is predicted. It is around two-thirds of the experimental value.

The estimation of the delamination area was conducted through the energy absorption formula (3) from Olsson. This estimation is better than the simple force-based approach by Poe but still does not provide a satisfactory result as the value is around 45% of the experimental value. This behavior is the same as expected and explained above for Poe's equation.

The layered-shell approach provides a force response prediction that is hardly better than the analytical curves. The model behaves much stiffer than the experiment. The insufficient progressive damage model of the layered-shell causes this behavior. The layered-shell elements have degrees of freedom only on the laminate level. The laminate theory couples all plies in their deformation behavior. Cracks in a single layer cannot open as the load is immediately transferred to the neighboring plies. For the same reason,
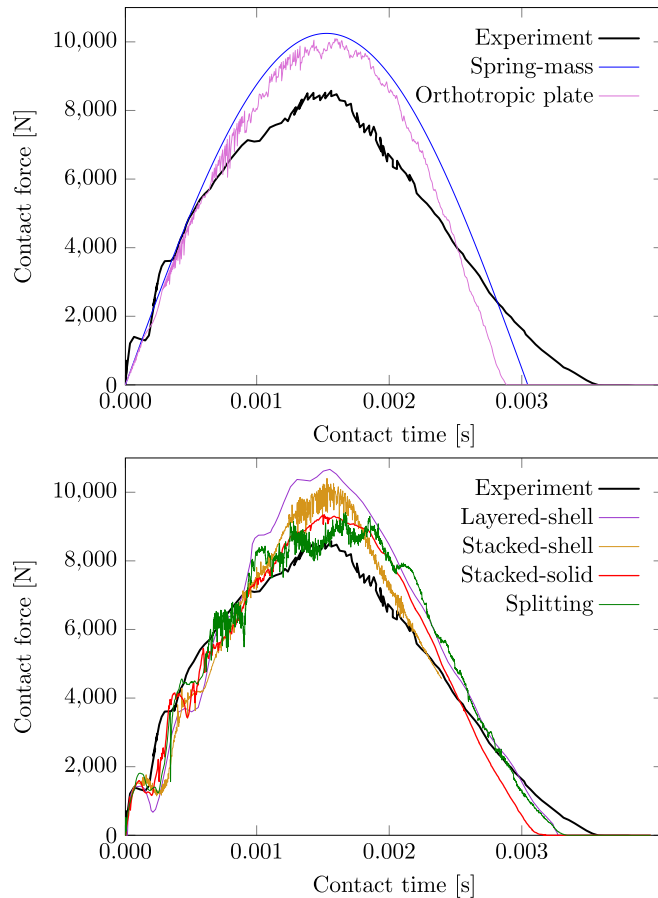
Fig. 11. Test case 1: Force-time history of analytical analysis methods (top) and FE simulations (down).

Table 5
Overview of predicted results and deviation from the test results for a 25 J impact on the layup A1 reported in Ref. [80].

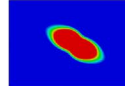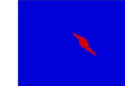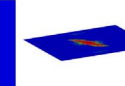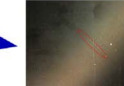|		Spring-mass	Ortho. plate	Layered-shell	Stacked-shell	Stacked-solid	Splitting	Test
F_{max}	[kN]	10.3 (+18%)	10.1 (+16%)	10.7 (+23%)	10.1 (+16%)	9.3 (+7%)	9.1 (+5%)	8.7
F_d	[kN]	4.4 (+16%)	4.4 (+16%)	4.6 (+21%)	5.3 (+1%)	5.0 (+1%)	5.20 (+1%)	3.8
d_{max}	[mm]	4.80 (−8%)	5.00 (−4%)	5.17 (±0%)	5.22 (±0%)	5.20 (±0%)	5.25 (+1%)	5.2
A_{dela}	[mm]	211 (−83%)	560 (−55%)	1650 (+33%)	963 (−23%)	1235 (−1%)	1110 (−9%)	1245
W_{dis}	[J]	–	8.0 (−36%)	5.3 (−58%)	6.0 (−52%)	6.5 (−48%)	7.6 (−39%)	12.5
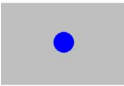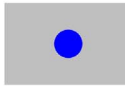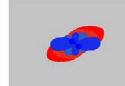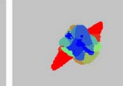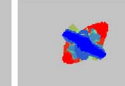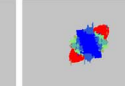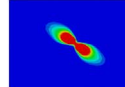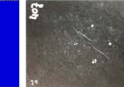
the predicted energy dissipation is not even half of the experimental value. In addition, the quantitative overprediction of the delamination area is likely to be caused by the overestimated contact force. However, the delamination results show qualitatively good agreement with the test.

With the *stacked-shell model*, the first meso-scale approach is evaluated. In comparison to the previous three results, the respective history curve is in better agreement with the experimental reference. However, the response still behaves too stiff. A possible explanation is the shell elements' insufficient prediction of the surface indentation behavior. Apart from the lowermost interface, the prediction of the delamination is plausible in shape, orientation, and size.

By the *stacked-solid model*, the prediction of the force history, the maximum force and the energy dissipation are improved. The curve still does not fit ideally, but it is much closer to the experimental reference. Also, the shape of the delaminations fits well to the test results — except the lowermost delamination which is underestimated. The most likely cause of this underestimation is a misbehavior of the interaction of tensile inter-fiber cracking and delamination. According to Choi and Chang [90] this interaction is crucial for predicting delamination in the interfaces on the impact backside.

Finally, the *splitting model* with the intra-ply cohesive zones is evaluated. Its predicted history curve is closely related to the result of the ordinary stacked-solid model. Differences can be observed in the delamination results. Even though their size and orientation is in agreement with the experimental results, the delaminations show a line pattern that results from the inter-fiber damage. The good fitting of the delamination results is only broken by the lowermost delamination. Even though the shape and the orientation are

Table 6
Damage modes of the second reference impact (40 J).

Inter-face	Spring-mass + Poe' seq.	Orth.plate + Olsson's eq.	Layered-shell	Stacked-shell	Stacked-solid	Splitting	Test result
Delami-nation	●	●	(image)	(image)	(image)	(image)	(image)
Fiber Crack	-	-	(image)	_a	(image)	(image)	(image)
Matrix Crack	-	-	(image)	_a	(image)	(image)	(image)

[a] Damage is computed internally by Abaqus Explicit but field output is not provided.
[b] Intralaminar cohesive elements are parallel to the z axis. Matrix cracks cannot be seen in the top view. A rotated view is used for the matrix cracks.

correctly captured, its extent is much too small.

In general, the data in Table 5 shows that the energy absorption is estimated too low by all the tested models. In literature, better agreements have been reported. Comparing the tested models in the present work with the reference models from other authors we need to point out one throughout difference: There is no permanent indentation considered in this work. Deformation occurs fully reversible. However, the prediction is sufficiently good for the loading phase, although the relaxation is not correctly reproduced. The energy that is dissipated through residual stresses after the impact is not considered in the value W_{dis} of all models. In addition, the
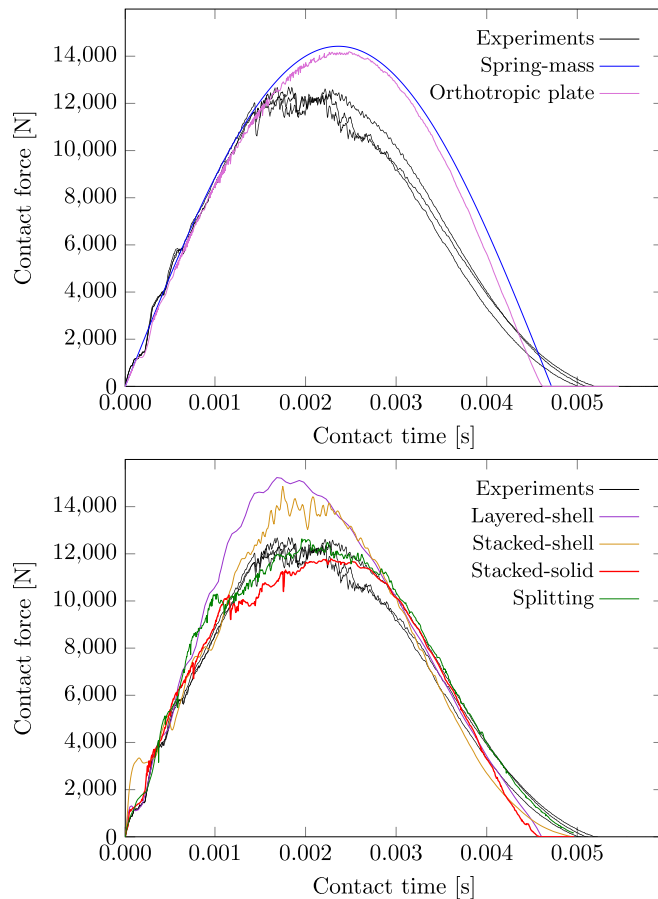

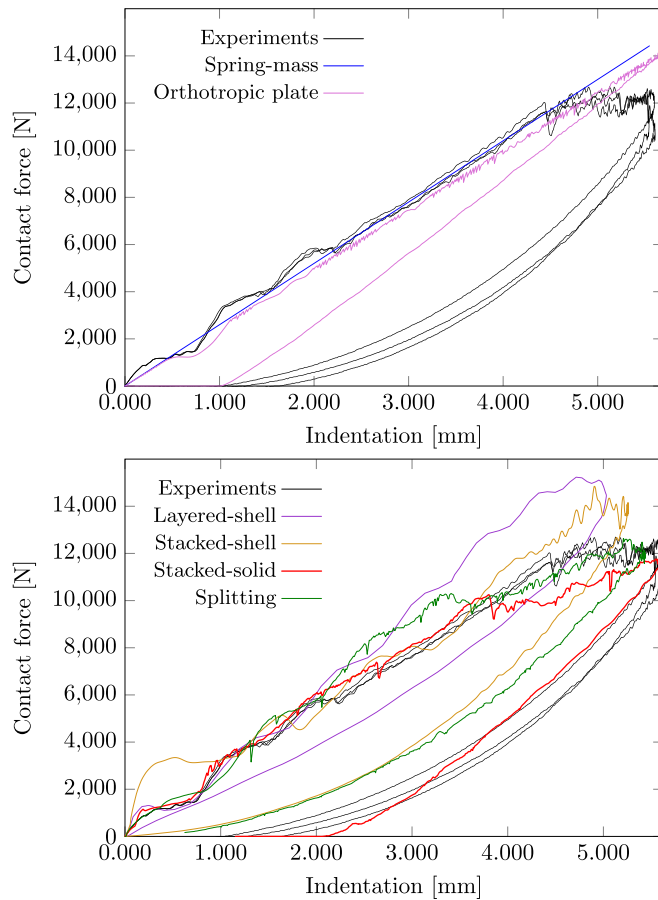**Fig. 12.** Test case 2: Force-time history of analytical analysis methods (top) and FE simulations (down).

Fig. 13. Test case 2: Force-displacement history of analytical analysis methods (top) and FE simulations (down).

Table 7
Overview of predicted results including the percentage of deviation from the test for a 40 J impact on the clustered layup from test case 2.

		Spring-mass	Ortho. plate	Layered-shell	Stacked-shell	Stacked-solid	Splitting	Test
F_{max}	[kN]	14.4 (+12%)	14.2 (+11%)	15.2 (+19%)	14.7 (+15%)	11.8 (−8%)	12.2 (−5%)	12.8 ± 0.3
F_d	[kN]	4.6 (−23%)	4.6 (−23%)	9.8 (+63%)	7.6 (+27%)	7.4 (+23%)	7.4 (+23%)	6.0 ± 0.3
d_{max}	[mm]	5.50 (+3%)	5.69 (+6%)	5.03 (−6%)	5.26 (−2%)	5.48 (+2%)	5.25 (−2%)	5.35 ± 0.12
T_i	[ms]	4.75 (−7%)	4.65 (−9%)	4.66 (−9%)	4.98 (−2%)	4.71 (−8%)	5.00 (−2%)	5.12 ± 0.16
A_{dela}	[mm²]	413 (−72%)	803 (−45%)	1680 (+16%)	1900 (+31%)	1650 (+14%)	1380 (−5%)	1450 ± 90
$l_{fibcrack}$	[mm]	–	–	(60)[b] (+3%)	–[a]	46 (−21%)	51 (−12%)	58 ± 8
$l_{matcrack}$	[mm]	–	–	(63)[b] (+15%)	–[a]	43 (−22%)	62 (+13%)	55 ± 5
W_{dis}	[J]	–	9.3 (−62%)	12.7 (−48%)	17.0 (−31%)	20.5 (−16%)	15.8 (−35%)	24.5 ± 1.9

[a] Damage is computed internally by Abaqus Explicit but field output is not provided.
[b] The simulation output is not a discrete crack but an area like the result in Table 6 shows.

compression damage behavior is not correctly captured by the bilinear law with fully elastic relaxation [3]. A plateau phase with a constant residual stress would lead to significant additional energy absorption.

However, also without the correct energy dissipation, plausible delamination shapes and good values for the projected delamination area are provided by all meso-scale FE models.

5.2.2. Test case 2: 40 J impact on a clustered laminate

In addition to the delamination, also fiber failure is present in this test case. The availability of more than one test result provides knowledge about the scatter of the test results. Analogously to test case 1, the results are presented in three parts: Table 6 contains a graphical overview of the impact damage results, the Figs. 12 and 13 show the history curves and Table 7 lists important quantitative values.

In contrast to test case 1, the delamination results are directly compared with the ultrasonic D-Scan image. Also, the fiber crack on the impact side and the inter-fiber crack on the back side are part of the comparison. Also, the force-displacement history in Fig. 13 is

plotted for this second test case. Each diagram contains experimental history curves of three experiments to allow an estimation of the simulation results in the context of experimental scatter.

The *analytical spring-mass model* shows a similar behavior like in the first test case. Before the force exceeds the threshold force for fiber failure at around 12 kN the approximation by the sine curve is quite good. But the lack of a progressive damage behavior leads to an overestimation of the contact force by more than 2 kN. Also the analytical damage prediction according to Poe's equation behaves similarly as for test case 1 and strongly underestimates the projected delamination area.

The *plate model* improves the contact force prediction hardly, in comparison with the spring-mass model. It neither captures the force drop after exceeding the fiber-failure threshold. However, it provides an energy dissipation of 9 J. Through Olsson's equation, this results in an estimation of the delamination area that is more than half of the test result.

The *layered-shell* approach also behaves similarly as in the previous test case. Its force response is too stiff, and the maximum is severely overestimated. The energy dissipation is with around 50% of the test result much too low. The delamination damage result is qualitatively suitable. However, it is worth mentioning that the delamination shapes are all of oval and do not show sharp edges like in the test. This lack of edges can also be traced back to the model's inability to emerge sublaminates and cracks in the laminate.

The *stacked-shell model* provides a significant improvement of the delamination pattern. Shape, size, and orientation of the visible damages fit well to the test result. Restricted by the capabilities of the built-in material model, the output of the computed intra-ply damage is not available and cannot be evaluated. The force history is still too stiff, and the force peak is overestimated by 2 kN. An improvement of the energy absorption to two-thirds of the experimental value indicates that the damage-modes are captured more realistically than with a macro-scale model.

Also for this test case, the *stacked-solid model* provides another step of improvement. The delamination pattern is well predicted. Also, the fiber crack and the matrix crack on the back side are captured plausibly. In contrast to the shell models, the force history fits better to the experimental curves. About the cohesive surfaces, one point is remarkable. With purely bilinear damage laws, this model is capable of predicting a permanent indentation value. This ability originates from the consideration of post-failure static friction by the cohesive surfaces [34]. This effect significantly improves the predicted energy dissipation which is now close to the test value.

Finally, the *splitting model* results confirm the impression of the first test case. The results are plausible regarding delamination, fiber failure, and inter-fiber cracking. A fringed delamination pattern, due to the in-plane cohesive zones, appears to be characteristic of this model. The force-time history shows a good fit in the loading phase. Only the relaxation is not captured perfectly due to the absence of a permanent indentation model in the cohesive elements. In comparison to the stacked-solid model, the energy absorption is lower. It is on the level of the layered-shell approach, which also uses cohesive elements.

5.3. Computational effort

Apart from the analysis results, the required computation effort is an important measure to assess an analysis method. For this benchmark, all simulations were conducted on the same computer system, a Linux cluster with 128 GB RAM and an Intel CPU Xeon E5-2690 with 3.8 GHz. Eight cores were used for each simulation with the Abaqus release 6.14-1.

Besides the number of finite elements and the impact duration, the maximum stable time increment Δt_{stable} plays a major role in the total computation effort of FE models. The stability of an explicit integration scheme is assessed with the Courant condition in Eq. (17). The dependency of the stable time increment on the smallest element length results in a high influence of the number of elements in the thickness direction. According to the Courant condition [91], the stable time increment increases proportionally with l_{crit} and reciprocally with the speed of wave propagation c_{wave}. c_{wave} results from the modulus E and the mass density ρ. For solid elements, the ply thickness t_{ply} determines this critical length.

$$\Delta t_{stable} \sim \frac{l_{crit}}{c_{wave}} \sim l_{crit} \sqrt{\frac{\rho}{E}}. \tag{17}$$

Regarding this condition for Δt_{stable}, the computation time $t_{compute}$ is influenced strongly by the laminate's ply thickness t_{ply}. This effect becomes even more severe when more than one element in thickness direction shall be used. Especially the analysis of composites of very thin plies is computational costly. If such thin plies or more than one element in thickness direction is required, a shell model could be an alternative for these plies.

Table 8
Computation effort for the first test case for all methods.

	Spring-mass	Plate	Layered-shell	Stacked-shell	Stacked-solid	Splitting
Elements [a]	–	–	5400	70,000	43,000	120,000
Integration points[b]	–	–	210,000	243,000	43,000	345,000
Computation time [h][c]	0	0.5	0.3	1.6	3.7	6.7

[a] Only elements of the composite specimen are taken into account. Impactor and support structure are modelled by 1750 additional elements.
[b] Three integration points per ply in thickness direction were chosen for shell elements.
[c] FE simulation run time on 8 CPUs for explicit and 2 CPUs for implicit time integration.

$$t_{compute} \sim \frac{n_{el}\,T_i}{\Delta t_{stable}} \sim \frac{n_{elZ}}{\frac{t_{ply}}{n_{elZ}}}$$

(18)

$$t_{compute} \sim n_{elZ}^2.$$

(19)

Implicit time integration is not affected by this instability issue. Transient simulation with much larger time increments is possible. But for another reason, its application on models with many degrees of freedom is not recommended. The computational effort per increment is increasing quadratically with the number of degrees of freedom. Its application to a meso-scale approach is accordingly not efficient. However, it is surely the right choice for a macro-scale approach. This approach requires only a few degrees of freedom, but many integration points. Therefore, it is efficient to use large increments. This avoids the evaluation of each integration point for a high number of increments like in an explicit simulation.

An overview about the computation time, the number of elements and integration points is given in Table 8. The spring-mass model requires only the evaluation of several analytical equations. Consequently, its computation effort is negligible. Although the plate model is still analytical, its transient evaluation needs to be performed with numerical time integration. With half an hour its computational effort already exceeds the effort for an FE macro-scale model. It is apparently visible that the computational effort increases strongly if a meso-scale method is applied. The corresponding large number of degrees of freedom requires several hours to achieve a simulation result. Especially the ply-splitting model has high computational costs. But also the stacked-solid model requires a larger computation time than the number of elements would suggest. The reason for the high computation time is the cohesive contact formulation, which does neither appear in the number of elements nor the number of integration points.

One remark about the layered-shell model needs to be added at this point. The corresponding computational effort was mainly driven by the included contact formulations between the impact setup and the specimen. Replacing these contact with boundary conditions reduces the computational effort drastically to less than 2 min.

5.4. Modeling aspects

A numerical or analytical impact analysis aims for the replacement of an impact test. Reduced costs, more flexibility, and faster results make numerical analysis attractive. However, these advantages are only a partial picture of the numerical analysis. In this subsection, we look at the analysis procedure comprehensively. This view goes beyond the actual impact analysis and considers the relocation of efforts.

The modeling effort around the analysis procedure consists of the required work for the preparation of the actual model and of the expenditure to determine the respective input parameters. In general, with increasing complexity of the model, the modeling effort also increases the preparation effort. Even though the modeling effort occurs only once per impact setup, for the analysis of a real use-case, parts of this effort will reoccur for each impact location. Therefore it can be a driving factor of a method's overall effort. The evaluation of the modeling aspects builds on the experiences of the authors during the research for behind this paper. Based on these experiences, this section includes brief elaborations of the most significant challenges related to the modeling and preparation procedure.

5.4.0.1. Impact setup and boundary conditions

An impact test, especially on coupon level, is conducted with a test setup that is in contact with the impact specimen. Replacing this test setup with boundary conditions strongly influences the indentation stiffness of the specimen. The damage is affected accordingly. If boundary conditions shall replace the model of the test setup, checking the elastic indentation stiffness is mandatory.

5.4.0.2. Material parameters

The replacement of impact testing effort through numerical analysis implies a relocation of the experimental effort to a lower level in the test pyramid [92]. Macro- and meso-scale methods require an elaborate material characterization. Parameters of the elasticity and the strengths of a unidirectional ply have to be determined. For the determination, in-plane parameters exist established standards. Difficulties arise with the determination of out-of-plane properties $E_{33}, G_{23}, X_{33c}, X_{23}$. Meso-scale models additionally need the critical energy release rates G as input values for the constitutive damage model. Standard tests are available for their determination at the ply interfaces. Comparable values for intra-ply damage are hard to obtain experimentally. For their determination, Pinho et al. [93] developed a test setup with a compact compression/tension specimen. However, the values reported in the literature are hardly traceable and diverge strongly for the fiber failure modes. For G_{f+} of unidirectional carbon fiber material, various authors report values between $101\frac{mJ}{mm^2}$ and $133\frac{mJ}{mm^2}$ [3,35,87,94]. The range for G_{f-} is similarly wide. During this benchmark, we experienced that the availability of these energy release rate is key for a good damage prediction. For that purpose, the calibration based on an impact test is an option [3].

The analytical spring-mass model requires either a similar test-based calibration or an accompanying elastic FE analysis. One calibration per impact configuration has to be performed. The plate model works with elastic parameters of a unidirectional ply. The plate stiffness constants of the classical laminate theory originate from these elastic parameters.

Concluding from this paragraph, the availability of material parameters can significantly influence the best-suited analysis method.

5.4.0.3. The choice of a finite element type

As impact load is an out-of-plane indentation, the laminate sees a significant bending load. As the mesh of macro-scale models describes the laminate as a whole, the elements have to be capable of capturing this bending. For that reason, shell elements are preferred on macro-scale. In contrast to that, the single plies see only slight bending. Compression on the impact side or tension on the impact backside dominates the state of stress in each ply. Accordingly, solid elements can be applied. These capture the out-of-plane strain and stresses, which is advantageous for capturing the local surface indentation of the impactor.

As the bending load can cause locking effects [95], reduced integrated elements are suitable in both macro and meso-scale models (S4R shell elements and C3D8R solid elements in Abaqus). These work with a single integration point per element, which facilitates the material degradation through a CDM model. In fully integrated elements with several integration points, damage can initiate at some of these points only while others remain intact. This disproportionality of stiffness between the integration points can result in severe element distortions which cause instability of the explicit simulation.

As linear reduced integrated elements tend to hourglassing, countermeasures have to be applied. Stiffness-based hourglass control or the enhanced option in Abaqus Explicit [81] are suitable for this purpose. In both cases, the artificial strain energy is an important measure to evaluate the validity of the solution. Its value has to remain small in comparison with the strain energy in the model.

Additionally, two other element types can be considered for application in meso-scale models. To avoid hourglassing, the incompatible mode elements (C3D8I in Abaqus) can be applied. These are fully integrated but suitable to capture bending deformation and can be applied to impact analysis [57]. However, they require a rectangular element shape. Alternatively, continuum shell elements (SC8R in Abaqus) are well-suited to capture bending load. These shell elements with eight nodes compute out-of-plane the strains from the nodal are computationally less expensive than solid elements [96] and their application for impact analysis was also studied [56].

5.4.0.4. Artificial parameters in cohesive zones

Meso-scale methods work with cohesive zones. These are well-suited for the prediction of delamination. However, their input parameters are not fully physically-based. The stiffness of a cohesive zone is a numerical parameter and makes a laminate softer than it would be. Extremely high stiffness values would affect the stable time increment of the simulation. Therefore a trade-off between artificial stiffness reduction by the cohesive zone and computational effort has to be made. According to Turon [73] this reduction shall not exceed two percent of the initial stiffness. Panettieri et al. [53] recommend to adjust the cohesive stiffness with the help of simple bending test cases.

Besides, the failure initiation in the cohesive zone requires strength parameters. This is an advantage of cohesive zones in comparison with other fracture mechanical approaches: it permits the combination of stress- and energy-based crack descriptions [97]. The exceedance of interfacial shear and normal strengths initiates the energy based crack propagation. However, only for a sufficiently fine mesh, these strength parameters are physical values. As we described in the Section 3.2 about cohesive zone methods, a minimum number of three elements is required in the cohesive zone of the crack tip. For a given element length, this requirement determines the artificial interface strength. Panettieri et al. investigated the influence of this numerical adaption on the delamination result of an impact analysis [53]. They observed a severe increase of the delamination area, for artificially reduced strengths values. Therefore, the element length in the cohesive zone and the strength parameters must be chosen with care. Otherwise, the impact solution could be affected.

5.4.0.5. Slave and master in contact formulations

Cohesive contact behavior can be applied only when a pure slave master formulation is used. Surface to surface contact is not available in the latest release of Abaqus Explicit. The slave and master sides must be chosen carefully. The laminate curvature under impact load can lead to severe penetrations of the plies if the inner contact partner forms the master surface. In contrast to that, the master surface on the outer contact partner does geometrically not allow a penetration of the inner partner's slave nodes (Fig. 14). Instead, gaps between the layers arise. While the first variant is too compliant, the latter is too stiff. Especially the higher compliance affects the structural behavior severely. Therefore the second option is chosen in this study.
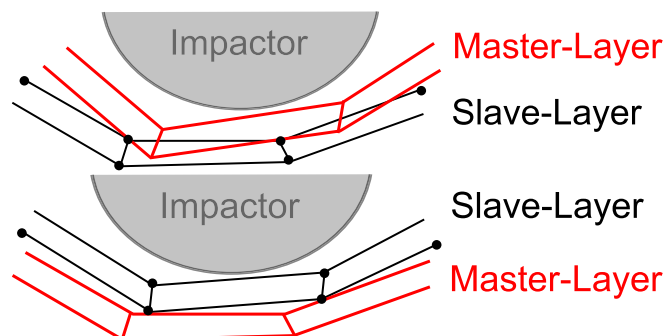

Fig. 14. Master-slave selection for neighbor plies under impact load.

5.4.0.6. Cohesive surface issues

Employing cohesive surfaces in a model differs from using cohesive elements. Although the model building itself is easier with cohesive surfaces, some additional conditions impede the analysis. An uneven master surface severely influences the damage behavior under compression load. Slave nodes that are close to a master element's edge tend to separate immediately if compression load is applied. This results in large, physically unlikely delaminations. Stability problems of the simulation are likely to arise. In consequence, incoherent meshes in neighboring plies must be applied. We found two possible solutions to this issue. Firstly, the slave surface can be equipped with a denser mesh. However, this solution cannot be employed for laminates because each embedded ply is simultaneously master for its upper and slave for its lower ply. The second solution is an adaption of the mesh. In each second ply, the nodes were shifted by 0.2 mm in the in-plane directions.

5.4.0.7. Intra-ply cohesive zones

Macro-scale modeling is fairly quick and easy, as the mesh only has to describe the mid plane of the laminate. Building up a meso-scale mesh is more costly. The stacking of the plies has to be arranged correctly. Many contact zones or tie constraints have to be defined. Cohesive surface modeling is still easier than building a model with cohesive elements. The latter have a finite thickness, and the ply thickness has to be reduced respectively. The ply properties can require adaption if the reduction is significant for the stress in the ply. However, up to that point, the model building can be well automatized. This changes when the ply-splitting model is implemented.

The cohesive zones in the ply-splitting model highly increase the modeling effort. Even on a flat plate, the fiber-aligned meshing is challenging if the fiber orientation differs from 0deg and 90deg. If a structural is not flat or not rectangular, a correctly aligned mesh becomes very hard to employ. Even though it is possible to create an appropriate model, the required building effort is likely to be inefficiently high.

5.4.0.8. Stacked-shells rotational degrees of freedom

A particular issue occurs when a stacked-shell model is combined with cohesive elements. The nodes of the shell elements have rotational degrees of freedom. The cohesive elements work with translational degrees of freedom only. Consequently, the deformation state of two neighboring plies is not fully coupled. This issue affects the specimen region close to the impact location. Here, the rotational amplitudes have their maximum values. As this area is relevant for the damage calculation, the overall result can be affected.

Uncoupled rotational deformation can occur in each ply on its own. The laminate is more compliant than it actually should be. Our rough estimations showed a reduction of the indentation stiffness by around two percent. The reduction is globally not severe, but the corresponding deformation concentrates on in the layer where the impactor it induces - on the impacted side. This can be observed in Fig. 15. In consequence, the structural effort is overestimated in the upper plies and underestimated on the impact backside. This finding is important when impact shall be analyzed through a stacked-shell method.

5.5. Conclusion of the coupon benchmark

Concluding the evaluation of effort and predictive capabilities, the six analyzed methods are qualitatively categorized in Fig. 16.

The *spring-mass model* can be used for a quick estimation of the expected values for contact force, impact duration and indentation. However, the corresponding damage prediction can hardly be compared with experimental results because a projected delamination area cannot be obtained. Also, a spring-mass model does not provide a real closed-form solution as it requires input about the indentation stiffness. The easiest methods to obtain this value are an FE simulation or an impact experiment.

The *plate model* is slightly improving the analysis results, but strongly increasing the analysis effort. Its advantage is only that it is a full closed-form solution and can work with stiffness parameters of the unidirectional plies. Anyway, it can hardly be used for plausible damage predictions.

A *layered-shell model* is probably the best compromise between the resulting quality and the computation effort. If contact modeling can be avoided, this method can be applied to obtain a plausible damage result quickly, even though the numerical model does not capture the damage mechanisms physically-sound.

The *stacked-shell approach* significantly increases the analysis effort. Although its modeling and computation are costly, a meso-
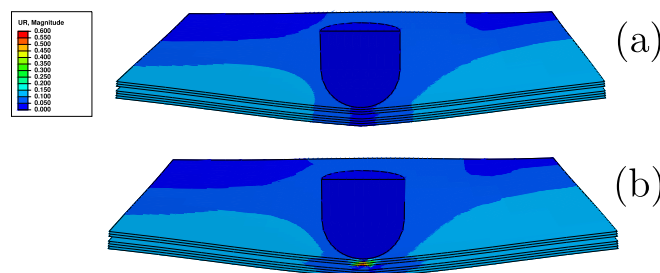

Fig. 15. Behavior of rotational degrees of freedom if coupling between the plies is applied (a) and omitted (b).
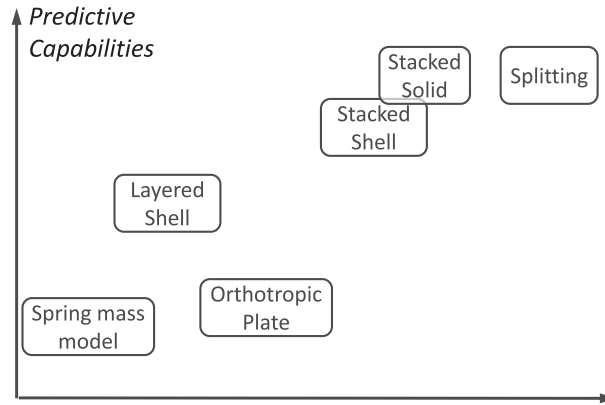
Fig. 16. Evaluation of the tested models as qualitative graphical illustration.

scale abstraction is required to provide satisfactory results for the impact response and the damage in the laminate. Shell elements are advantageous for very thin plies, as their stable time increment is not affected by the ply thickness.

The *stacked-solid model* still improves of the capturing of surface indentation by the impactor and hardly increases the expenses. Therefore this approach should be preferred to a stacked-shell model. Also, the application of cohesive surfaces instead of cohesive elements has an impact on the model. On the one hand, the cohesive surfaces even lower the modeling effort but on the other hand, they increase the computational effort. In addition, cohesive surfaces allow considering permanent indentation by static friction, which is a significant improvement.

Including *splitting* in the model improves the physical soundness of the meso-scale approach. However, it strongly increases the computation and modeling effort. The results of this model are comparable to an ordinary stacked-solid approach. Accordingly, its superior advantages could not be confirmed in this study. Regarding a less-advanced meso-scale model, losses in accuracy and sensitivity of the model can be accepted, but the modeling and computation are much lower.

6. Application on the structural level

The conducted benchmark proofs the capability of several methods to achieve a plausible result. For physically-sound damage behavior, the application of a meso-scale method is appropriate. At the same time, the large computational effort for small specimens makes a direct transfer to the structural level unattractive. Confirming the result from the literature review in Section 2, the authors conclude that the computation effort of an accurate meso-scale model is too large for their direct application on the structural level. Only a layered-shell model could be considered for immediate application. However, the applicability of high-fidelity simulation methods can severely be improved by exploiting some characteristics of low-velocity impact:

6.1. Local damage

LVI damage is likely to occur locally in the contact zone with the impactor. It seems reasonable to establish a global-to-local
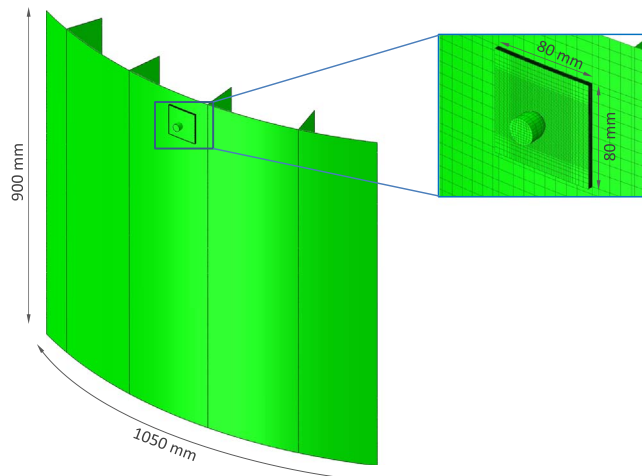

Fig. 17. Generic composite panel for evaluation of the computation effort on structural level.

Table 9
Computation effort on structural level.

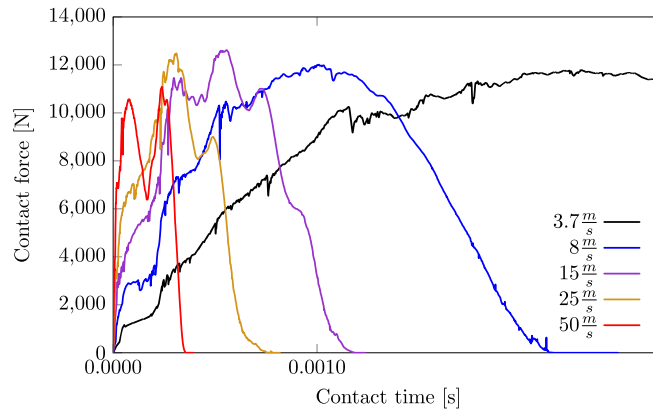|	Layered shell	Stacked-solid	Coupled mesh	CAI stacked-solid
Computation time [h]	0.3	208	5.7	3.7

Fig. 18. Simulated force history of the 40 J impact in test case 2 with changed impactor velocity and mass.

approach. Reducing the analysis zone for the high-fidelity model significantly decreases the computation effort for a structure. The most simple realization would be a direct integration of the meso-scale mesh in a coarse macro-scale mesh. Implemented by Schwab [98] and Riccio [66], the suitability of this approach has been proven. Accordingly, a substructure model could be applied, making a superelement from the surrounding structure of the damage relevant impact zone.

For evaluation of the computation effort of a structure in comparison to the benchmarked coupons, impact simulations on a generic stiffened panel as illustrated in Fig. 17 are conducted. Outer dimensions of 1050×900 mm^2, a curvature radius of 1200 mm and the layup of test case 2 are employed. The panel was meshed three times, using layered-shells, a high-fidelity stacked-solid, and a coupled mesh. The associated computation times are listed in Table 9 and compared to the stacked-solid model on CAI level. While a layered-shell simulation can easily be conducted on a structure, the stacked-solid model results in an inefficiently high effort. Additionally, the application of a biased mesh results in elements with very poor aspect ratio, possibly resulting in numerical difficulties. By a coupled mesh model, the computational effort only slightly exceeds the effort on coupon level. The computation effort for structural LVI simulation is driven by the damage-prone area, which requires a meso-scale mesh to capture a plausible progressive damage behavior. This procedure is legitimate if impact damage occurs only locally. Even though this is quite likely for low-velocity impact, if non-local damage would occur anyway, the simplified model runs the risk of missing it. At this point, it is important to keep attention on possible damage hot spots around the impact location. An appropriate layered-shell model becomes important. The coupon benchmark has shown the capability to predict damage by layered-shells, even though the progressive damage behavior is insufficient. Using this capability, the surrounding structure around the impact zone can be checked for possible damage prone areas, using a simple shell model and a suitable failure condition.

6.2. Increased impactor velocity

In the work of Abisset [52], the equivalence of LVI damage and quasistatic indentation was determined. This equivalence reversely leads to an additional similarity of impact scenarios. Keeping the impact energy constant, the variation of impactor velocity and mass will not affect the damage result. Exploiting the range of similarity, speeding up an LVI scenario becomes possible by reducing the impactor weight and increasing its initial velocity. This adjustment firstly affects the impact duration in the force-time history, as shown in Fig. 18. Anyway, speeding up the impact process does not necessarily lead to relevant differences in the damage effects. A look at the force-displacement curve supports a possible similitude (Fig. 19). Both figures compare the history data of high-fidelity impact simulations of the same specimen impacted with a constant energy of 40 J but different impactor velocities between $3.7 \frac{m}{s}$ and $50 \frac{m}{s}$. The mass was chosen accordingly.

LVI is driven by the quasistatic response of a structure [8]. In the dynamic impact system, this response is in agreement with the first system's eigenmode. Relevant participation of higher order eigenmodes indicates the end of the LVI zone, where a changed damage behavior is likely to occur. The physical damage cause and the result become invalid for the actual reference of LVI. Therefore the authors additionally conducted a modal analysis and analyzed the energy distribution over the system's eigenmodes[3]. From the high-fidelity analysis and the modal analysis, the following possible limitation factors were identified:

---

[3] Modal analysis of the impact system was conducted by tying contact points of the specimen with impactor and support structure.
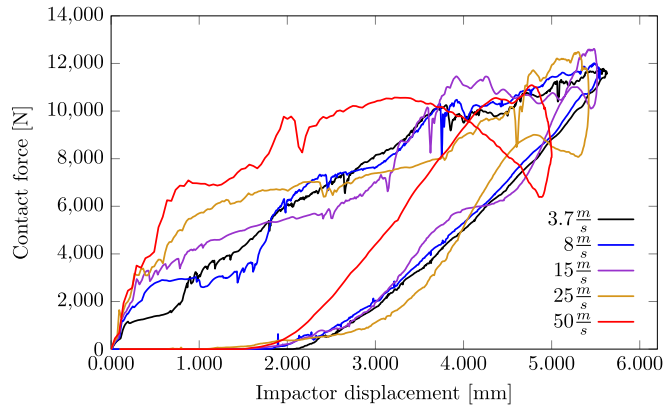
Fig. 19. Simulated force-displacement history of the 40 J impact in test case 2 with changed impactor velocity and mass.

Table 10
Eigenmodes of impact systems with changed impactor velocity and mass.

	3.7 $\frac{m}{s}$	8 $\frac{m}{s}$	15 $\frac{m}{s}$	25 $\frac{m}{s}$	50 $\frac{m}{s}$
Eigen-frequencies	I. 136 Hz	297 Hz	555 Hz	939 Hz	1707 Hz
	II. 5661 Hz	5668 Hz	5691 Hz	5754 Hz	5880 Hz
Energy in mode I[a]	99.9%	99.7%	98.4%	95.7%	83.5%
Mode I					
Mode II					
Dela-mination					

[a] Ratio of energy in mode I to total impact energy.

- Changed eigenmode shapes
- Energy fraction in higher order vibration modes
- Different damage threshold force or maximum contact force
- Different damage pattern

The influence of higher order vibrations is usually driven by the second eigenmode. Its effect is visible in the force history of all five analyzed impact systems. Its frequency is nearly independent from the impactor mass (compare with Table 10 and Fig. 11). But the increasing frequency of the first mode reduces the gap to the second eigenmode. While the shape of the first mode remains unaffected on the entire velocity range, the second mode shows first differences only above $25\frac{m}{s}$.

Regarding the influence of the energy distribution, a theoretical assumption is made: Based on Olsson's assessment of LVI, only the deformation of the first mode is considered damage relevant. Energy in other eigenmodes is not contributing to the damage. A decreasing energy fraction in the first mode would reduce the effective impact energy. Analogously to the limit for artificial energy in an FE model, an energy limit of around three percent could be defined here. Reversely, at least 97% of energy should go to mode one. This limit is conservative, as the energy in higher order modes is likely to propagate damage, too. Consequently, the actual effective impact energy can be considered higher than the fraction in the first mode.

Additionally, the influence of the varying impactor mass on force thresholds and the maximum contact force has to be taken into

account. A significantly changed damage threshold like it occurred in the simulation with $50\frac{m}{s}$ is likely to involve a different damage-mode or location. Qualitative change of the damage result can be expected. The maximum contact force is a driving factor for the damage propagation [16]. A relevant change of the maximum value would primarily affect the damage quantitatively. Regarding the force history curves, the influence of higher-order vibration fades away for $3.7\frac{m}{s}$ and $8\frac{m}{s}$. In the simulation with $15\frac{m}{s}$, a constant oscillation remains in the system, possibly influencing the maximum contact force by its amplitude. This observation suggests a limit between the configurations $8\frac{m}{s}$ and $15\frac{m}{s}$.

While the previous limitation factors are physically based, the damage pattern is a phenomenological factor. If any physical limits are exceeded, the damage pattern works as an indicator. Between the five impact configuration, a significant influence is visible for $25\frac{m}{s}$ and above. This indicates that the limit of validity is located around the $15\frac{m}{s}$ configuration. Influence on the force history is recognizable, anyway the damage pattern is still unaffected. The mode shapes and the modal energy distribution still conform to the limits. In the given example (test case 2) the contact time reduces by factor three between $3.7\frac{m}{s}$ and $15\frac{m}{s}$. The computational effort decreases proportionally.

In that range, the energy ratio of the first eigenmode is still very high. It receives 98% of the total impact energy. This is enough to consider the missing two percent negligible for damage development but obviously more than in the reference case of the experimental impact with $3.7\frac{m}{s}$. The trend of this energy ratio can additionally be exploited. Indicating the validity of an accelerated impact, it defines the LVI limit for an arbitrary impact system. While a definition according to velocity or impactor mass does not take into account the structural response, the derived criterion, called *Mode One Energy Ratio*, can serve as an objective measure of the characteristics of an impact system. The conducted analysis suggests a limit between one and a half and two percent of the total energy to be allowed in higher order vibration modes.

7. Conclusion and outlook

The conducted review and benchmark of methods on different abstraction scales showed that impact simulation is still a challenge. Within the presented FE methods, even simple models are capable of predicting the major damage-modes of LVI. Anyway, not all of them use physically correct damage behavior. For a quick estimation, the application of a macro-scale model with layered-shell elements is recommended. In this case, contact modeling should be avoided and implicit time integration is the right choice.

To achieve better damage results, we recommend applying a meso-scale approach. The modeling effort and the computation effort are much higher than for a layered-shell model, but the impact process and its damage are captured physically plausible. Cohesive surfaces and finite solid elements are the suggested choice, concluding this study.

For further improvement of the results, advanced damage-models are required. Permanent indentation, nonlinear shear behavior, and the constitutive law for full compression damage must be taken into account. Although such approaches are not part of this study, it is important to mention that the most models in recent publications contain these advances. Their implementation to any of the presented models in this study is possible.

Impact simulation on composite structures can be conducted with comparable computation effort as coupons. Local analysis approaches with increased impact velocity are the key to achieve structural impact analysis in a manageable time frame. If a high-fidelity model of sufficient accuracy can be established, it will not make tests redundant but move the testing to a lower level in the testing pyramid. Many material parameters, especially for fracture mechanics, have to be determined experimentally. With the degree of detail also the number of required parameters increases. Especially cohesive zone approaches require additional parameters that depend on physical and numerical properties. Their definition itself is an object of research.

This results in an additional aspect for best choice of a simulation method — the availability of material parameters. High-fidelity methods require a large set of parameters for elasticity, strength and damage behavior. Especially the latter is often not available. In that case, the application of a layered-shell model should be preferred, as the progressive damage behavior is unlikely to be predicted correctly. If there is also no strength data available, the application of analytical analysis in combination with the evaluation of threshold forces can be a good alternative.

The analysis of impact on the structural level is the next important step. LVI damage itself is not concerning the entire structure but is rather a local phenomenon. A large part of the impacted structure is only participating in the impact by elastic deformation. A detailed damage-model is not required in this region. A combination of stacked layer and layered-shell model appears to be the best choice for these scenarios. The surrounding framework of the damage-prone area is sufficiently described by shell elements without progressive damage-model. The evaluation of failure conditions is sufficient to ensure the validity of the chosen damage zone and determine other points of possible damage.

Finally, the possible acceleration of impact simulations by increasing the impactor speed and reducing its mass allows reducing the computational effort significantly. The acceleration is limited when the impact system leaves the LVI range. To determine this limit objectively, an energy-based criterion was derived, the *Mode I Energy Ratio*. It uses the energy fraction of the first eigenmode and the total impact energy. If this is at least 98%, an impact system complies the assumptions of LVI. Respecting the properties of the entire impact system, this criterion is superior to definitions based on mass and velocity of the impactor.

Acknowledgements

References

[1] D. Liu, E. Lansing, L.E. Malvern, Cracking in impacted glass/epoxy plates, J. Compos. Mater. 21 (July 1987) (1987) 594–609.

[2] M. Richardson, M. Wisheart, Review of low-velocity impact properties of composite materials, Compos. Part A Appl. Sci. Manuf. 27 (12) (1996) 1123–1131 http://linkinghub.elsevier.com/retrieve/pii/1359835X96000747http://dx.doi.org/10.1016/1359-835X(96)00074-7.

[3] W. Tan, B.G. Falzon, L.N. Chiu, M. Price, Predicting low velocity impact damage and Compression-After-Impact (CAI) behaviour of composite laminates, Compos. Part A Appl. Sci. Manuf. 71 (2015) 212–226 http://linkinghub.elsevier.com/retrieve/pii/S1359835X15000366http://dx.doi.org/10.1016/j.compositesa.2015.01.025.

[4] S. Abrate, Impact on laminated composite materials, Appl. Mech. Rev. 44 (4) (1991) 155–190, http://dx.doi.org/10.1115/1.3119500.

[5] E. González, P. Maimí, P.P. Camanho, A. Turon, J. Mayugo, Simulation of drop-weight impact and compression after impact tests on composite laminates, Compos. Struct. 94 (11) (2012) 3364–3378 http://linkinghub.elsevier.com/retrieve/pii/S0263822312002309http://dx.doi.org/10.1016/j.compstruct.2012.05.015.

[6] A.P. Christoforou, A.S. Yigit, Effect of flexibility on low velocity impact response, J. Sound Vib. 217 (3) (1998) 563–578 http://linkinghub.elsevier.com/retrieve/pii/S0022460X98918077http://dx.doi.org/10.1006/jsvi.1998.1807.

[7] A.P. Christoforou, Impact dynamics and damage in composite structures, Compos. Struct. 52 (2) (2001) 181–188, http://dx.doi.org/10.1016/S0263-8223(00)00166-5.

[8] R. Olsson, Analytical prediction of large mass impact damage in composite laminates, Compos. Part A Appl. Sci. Manuf. 32 (9) (2001) 1207–1215, http://dx.doi.org/10.1016/S1359-835X(01)00073-2.

[9] R. Olsson, Analytical model for delamination growth during small mass impact on plates, Int. J. Solids Struct. 47 (21) (2010) 2884–2892, http://dx.doi.org/10.1016/j.ijsolstr.2010.06.015.

[10] H. Singh, P. Mahajan, Analytical modeling of low velocity large mass impact on composite plates including damage evolution, Compos. Struct. 149 (2016) 79–92 http://www.sciencedirect.com/science/article/pii/S0263822316302495http://dx.doi.org/10.1016/j.compstruct.2016.04.009.

[11] A.L. Dobyns, Analysis of simply-supported orthotropic plates subject to static and dynamic loads, AIAA. J. 19 (5) (1981) 642–650, http://dx.doi.org/10.2514/3.50984.

[12] R. Olsson, Impact response of orthotropic composite plates predicted from a one-parameter differential equation, AIAA J. 30 (6) (1992) 1587–1596, http://dx.doi.org/10.2514/3.11105.

[13] S.R. Swanson, Contact deformation and stress in orthotropic plates, Compos. Part A Appl. Sci. Manuf. 36 (2005) 1421–1429, http://dx.doi.org/10.1016/j.compositesa.2004.11.011.

[14] F. Najafi, M.H. Shojaeefard, H. Saeidi Googarchin, Low-velocity impact response of functionally graded doubly curved panels with Winkler-Pasternak elastic foundation: an analytical approach, Compos. Struct. 162 (2016) 351–364 http://www.sciencedirect.com/science/article/pii/S0263822316312612http://dx.doi.org/10.1016/j.compstruct.2016.11.094.

[15] G. Schoeppner, S. Abrate, Delamination threshold loads for low velocity impact on composite laminates, Compos. Part A Appl. Sci. Manuf. 31 (9) (2000) 903–915 http://www.sciencedirect.com/science/article/pii/S1359835X00000610http://dx.doi.org/10.1016/S1359-835X(00)00061-0.

[16] W.C. Jackson, C.C. Poe, The Use of Impact Force As a Scale Parameter for the Impact Response of Composite, Tech. Rep. NASA Langley Reseach Center, Hampton, Virginia, 1992.

[17] D. Elder, R. Thomson, M. Scott, Comparison of composite damage predictions between a 2D, 3D LS-Dyna simulation and experimental results for a low speed impact event, Proc. Tenth aust. Int. Aerosp. Congr., Brisbane, 2003.

[18] J. Yap, M. Scott, D. Hachenberg, J. Baaran, Composite stiffened panels impact damage simulation and parametric studies, Proc. Tenth aust. Int. Aerosp. Congr., Brisbane, 2003.

[19] J. Baaran, L. Kärger, a. Wetzel, Efficient prediction of damage resistance and tolerance of composite aerospace structures, Proc. Inst. Mech. Eng. Part G J. Aerosp. Eng. 222 (2) (2008) 179–188 http://journals.pepublishing.com/openurl.asp?genre=article&id=http://dx.doi.org/10.1243/09544100JAERO278http://dx.doi.org/10.1243/09544100JAERO278.

[20] L. Kärger, J. Baaran, J. Teßmer, Efficient simulation of low-velocity impacts on composite sandwich panels, Comput. Struct. 86 (9) (2008) 988–996 http://linkinghub.elsevier.com/retrieve/pii/S0045794908000151http://dx.doi.org/10.1016/j.compstruc.2007.04.029.

[21] L. Kärger, J. Baaran, A.J. Gunnion, R. Thomson, Evaluation of impact assessment methodologies. Part I: applied methods, Compos. Part B Eng. 40 (1) (2009) 65–70 http://linkinghub.elsevier.com/retrieve/pii/S1359836808000863http://dx.doi.org/10.1016/j.compositesb.2008.06.003.

[22] A.F. Johnson, A.K. Pickett, P. Rozycki, Computational methods for predicting impact damage in composite structures, Compos. Sci. Technol. 61 (15) (2001) 2183–2192, http://dx.doi.org/10.1016/S0266-3538(01)00111-7.

[23] O. Allix, P. Ladevèze, Interlaminar interface modelling for the prediction of laminate delamination, Compos. Struct. 22 (1992) 235–242.

[24] A.S. Kaddour, M.J. Hinton, Maturity of 3D failure criteria for fibre-reinforced composites: comparison between theories and experiments: part B of WWFE-II, J. Compos. Mater. 47 (6-7) (2013) 925–966 http://jcm.sagepub.com/content/47/6-7/925%5Cnhttp://jcm.sagepub.com/content/47/6-7/925.abstracthttp://dx.doi.org/10.1177/0021998313478710.

[25] K. Rohwer, Predicting fiber composite damage and failure, J. Compos. Mater. 1 (September) (2014), http://jcm.sagepub.com/content/early/2014/09/26/0021998314553885.abstract http://dx.doi.org/10.1177/0021998314553885 0021998314553885–.

[26] R. Borg, L. Nilsson, K. Simonsson, Simulation of delamination in fiber composites with a discrete cohesive failure model, Compos. Sci. Technol. 61 (5) (2001) 667–677, http://dx.doi.org/10.1016/S0266-3538(00)00245-1.

[27] R. Borg, L. Nilsson, K. Simonsson, Simulation of low velocity impact on fiber laminates using a cohesive zone based delamination model, Compos. Sci. Technol. 64 (2) (2004) 279–288 http://linkinghub.elsevier.com/retrieve/pii/S0266353803002562http://dx.doi.org/10.1016/S0266-3538(03)00256-2.

[28] M. Loikkanen, G. Praveen, D. Powell, Simulation of ballistic impact on composite panels, 10th Int. LS-DYNA Conf. (2008) 1–12, http://dx.doi.org/10.15632/jtam-pl.53.2.263.

[29] C. Bouvet, S. Rivallant, J.J. Barrau, Modelling of impact damage and permanent indentation on laminate composite plate, 14th Eur. Conf. Compos. Mater. (June) (2010) 1–10.

[30] B.A. Gama, J.W. Gillespie Jr, Finite element modeling of impact, damage evolution and penetration of thick-section composites, Int. J. Impact Eng. 38 (4) (2011) 181–197 http://www.sciencedirect.com/science/article/pii/S0734743X1000196Xhttp://dx.doi.org/10.1016/j.ijimpeng.2010.11.001.

[31] Y. Shi, C. Pinna, C. Soutis, Modelling impact damage in composite laminates: a simulation of intra- and inter-laminar cracking, Compos. Struct. 114 (2014) 10–19 http://linkinghub.elsevier.com/retrieve/pii/S026382231400155Xhttp://dx.doi.org/10.1016/j.compstruct.2014.03.052.

[32] P.F. Liu, B.B. Liao, L.Y. Jia, X.Q. Peng, Finite element analysis of dynamic progressive failure of carbon fiber composite laminates under low velocity impact, Compos. Struct. 149 (2016) 408–422, http://dx.doi.org/10.1016/j.compstruct.2016.04.012.

[33] C. Bouvet, N. Hongkarnjanakul, S. Rivallant, J.-j. Barrau, Discrete impact modeling of inter- and intra-laminar failure in composites, Dyn. Fail. Compos. Sandw. Struct. 192 (2013) 339–392, http://dx.doi.org/10.1007/978-94-007-5329-7.

[34] C. Lopes, S. Sádaba, C. González, J. Llorca, P.P. Camanho, Physically-sound simulation of low-velocity impact on fibre reinforced laminates, Int. J. Impact Eng. (2015) 1–15 http://www.sciencedirect.com/science/article/pii/S0734743X15001128http://dx.doi.org/10.1016/j.ijimpeng.2015.05.014.

[35] A. Riccio, S. Saputo, A. Sellitto, V. Lopresto, Characterisation of the impact induced damage in composites by cross-comparison among experimental non-destructive evaluation techniques and numerical simulations, Proc. Inst. Mech. Eng. Part C J. Mech. Eng. Sci. 0 (0) (2016), http://dx.doi.org/10.1177/0954406216681595 0954406216681595.

[36] R. Bogenfeld, J. Kreikemeier, A tensorial based progressive damage model for fiber reinforced polymers, Compos. Struct. 168 (2017) 608–618, http://dx.doi.org/10.1016/j.compstruct.2017.02.006.

[37] E. Panettieri, D. Fanteria, M. Montemurro, C. Froustey, Low-velocity impact tests on carbon/epoxy composite laminates: a benchmark study, Compos. Part B Eng. 107 (2016) 9–21, http://dx.doi.org/10.1016/j.compositesb.2016.09.057.

[38] B.Z. Haque, A Progressive Damage Model for Unidirectional and Woven Fabric Composites, Tech. Rep. May, University of Delaware Center for Composite Materials, Delaware, 2014.

[39] S. Rivallant, C. Bouvet, N. Hongkarnjanakul, Failure analysis of CFRP laminates subjected to compression after impact: FE simulation using discrete interface elements, Compos. Part A Appl. Sci. Manuf. 55 (2013) 83–93 http://linkinghub.elsevier.com/retrieve/pii/S1359835X13002273http://dx.doi.org/10.1016/j.compositesa.2013.08.003.

[40] G. Nian, Y. Shan, Q. Xu, S. Qu, Q. Yang, Failure analysis of syntactic foams: a computational model with cohesive law and XFEM, Compos. Part B Eng. 89 (2016) 18–26, http://dx.doi.org/10.1016/j.compositesb.2015.10.044.

[41] S. Chen, M. Zang, D. Wang, S. Yoshimura, T. Yamada, Numerical analysis of impact failure of automotive laminated glass: a review, Compos. Part B Eng. 122 (2017) 47–60 http://www.sciencedirect.com/science/article/pii/S1359836816328384http://dx.doi.org/10.1016/j.compositesb.2017.04.007.

[42] G. Molnár, A. Gravouil, 2D and 3D Abaqus implementation of a robust staggered phase-field solution for modeling brittle fracture, Finite Elem. Anal. Des. 130 (November 2016) (2017) 27–38 http://linkinghub.elsevier.com/retrieve/pii/S0168874X16304954http://dx.doi.org/10.1016/j.finel.2017.03.002.

[43] Y. Huang, L. Xu, S. Kyu Ha, Prediction of three-dimensional composite laminate response using micromechanics of failure, J. Compos. Mater. 46 (June) (2012) 2431–2442, http://dx.doi.org/10.1177/0021998312449888.

[44] R. von Mises, Mechanik der festen Körper im plastisch deformablen Zustand, Nachr. Ges. Wiss. Goettingen 1 (1913) 582–592.

[45] D. Krause, A physically based micromechanical approach to model damage initiation and evolution of fiber reinforced polymers under fatigue loading conditions, Compos. Part B Eng. 87 (2016) 176–195, http://dx.doi.org/10.1016/j.compositesb.2015.10.012.

[46] C. Lopes, S. Sadaba, F. Naya, C. González, Multiscale Simulation Strategy for Low-Velocity Impact on FRP, in: R.K. Hyonny Kim, D. Whisler, Z.M. Chen, C. Bisagni, M. Kawai (Eds.), Proc. Am. Soc. Compos. - 29th Tech. Conf. Compos. Mater. DEStech Publications, Inc, 2014, pp. 59–78.

[47] D. Ivančević, I. Smojver, Explicit multiscale modelling of impact damage on laminated composites Part I: validation of the micromechanical model, Compos. Struct. 145 (2016) 248–258 http://linkinghub.elsevier.com/retrieve/pii/S0263822316300897http://dx.doi.org/10.1016/j.compstruct.2016.02.048.

[48] S. Abrate, Impact on Composite Structures, Cambridge University Press, Cambridge, 1998.

[49] D.J. Elder, R.S. Thomson, M.Q. Nguyen, M.L. Scott, Review of delamination predictive methods for low speed impact of composite laminates, Compos. Struct. 66 (1-4) (2004) 677–683, http://dx.doi.org/10.1016/j.compstruct.2004.06.004.

[50] P. Jousset, M. Rachik, Comparison and evaluation of two types of cohesive zone models for the finite element analysis of fracture propagation in industrial bonded structures, Eng. Fract. Mech. 132 (2014) 48–69, http://dx.doi.org/10.1016/j.engfracmech.2014.10.018.

[51] M. May, Numerical evaluation of cohesive zone models for modeling impact induced delamination in composite materials, Compos. Struct. 133 (2015) 16–21 http://www.sciencedirect.com/science/article/pii/S0263822315005760http://dx.doi.org/10.1016/j.compstruct.2015.07.032.

[52] X. Sun, M. Wisnom, S. Hallett, Interaction of inter- and intralaminar damage in scaled quasi-static indentation tests: part 2 — numerical simulation, Submitt. to Compos. Struct. 136 (2015) 712–726, http://dx.doi.org/10.1016/j.compstruct.2015.09.061.

[53] E. Panettieri, D. Fanteria, F. Danzi, Delaminations growth in compression after impact test simulations: influence of cohesive elements parameters on numerical results, Compos. Struct. 137 (2016) 140–147, http://dx.doi.org/10.1016/j.compstruct.2015.11.018.

[54] H. Singh, P. Mahajan, Modeling damage induced plasticity for low velocity impact simulation of three dimensional fiber reinforced composite, Compos. Struct. 131 (2015) 290–303 http://www.sciencedirect.com/science/article/pii/S0263822315003761http://dx.doi.org/10.1016/j.compstruct.2015.04.070.

[55] J. Pernas-Sánchez, J.A. Artero-Guerrero, J. Zahr Viñuela, D. Varas, J. López-Puente, Numerical analysis of high velocity impacts on unidirectional laminates, Compos. Struct. 107 (2014) 629–634, http://dx.doi.org/10.1016/j.compstruct.2013.08.035.

[56] S. Heimbs, T. Bergmann, D. Schueler, N. Toso-PentecÔte, High velocity impact on preloaded composite plates, Compos. Struct. 111 (1) (2014) 158–168, http://dx.doi.org/10.1016/j.compstruct.2013.12.031.

[57] H. a. Israr, S. Rivallant, C. Bouvet, J.J. Barrau, Finite element simulation of 0/90 CFRP laminated plates subjected to crushing using a free-face-crushing concept, Compos. Part A Appl. Sci. Manuf. 62 (2014) 16–25, http://dx.doi.org/10.1016/j.compositesa.2014.03.014.

[58] B. Falzon, P. Apruzzese, Numerical analysis of intralaminar failure mechanisms in composite structures. Part I: FE implementation, Compos. Struct. 93 (2) (2011) 1039–1046 http://www.sciencedirect.com/science/article/pii/S0263822310002370http://dx.doi.org/10.1016/j.compstruct.2010.06.028.

[59] C. Bouvet, S. Rivallant, J.J. Barrau, Low velocity impact modeling in composite laminates capturing permanent indentation, Compos. Sci. Technol. 72 (16) (2012) 1977–1988, http://dx.doi.org/10.1016/j.compscitech.2012.08.019.

[60] H. Hertz, Ueber die Berührung fester elastischer Körper, J. Reine Angew. Math. I (92) (1881) 156–171, http://dx.doi.org/10.1515/crll.1882.92.156.

[61] D.H. Li, Y. Liu, X. Zhang, Low-velocity impact responses of the stiffened composite laminated plates based on the progressive failure model and the layerwise/solid-elements method, Compos. Struct. 110 (Good paper) (2014) 249–275, http://dx.doi.org/10.1016/j.compstruct.2013.12.011 IwillfindtheURL.

[62] B. Falzon, P. Apruzzese, Numerical analysis of intralaminar failure mechanisms in composite structures. Part I: FE implementation, Compos. Struct. 93 (2) (2011) 1039–1046 http://www.sciencedirect.com/science/article/pii/S0263822310002370http://dx.doi.org/10.1016/j.compstruct.2010.06.028.

[63] D. Fanteria, G. Longo, E. Panettieri, A non-linear shear damage model to reproduce permanent indentation caused by impacts in composite laminates, Compos. Struct. 111 (1) (2014) 111–121, http://dx.doi.org/10.1016/j.compstruct.2013.12.017.

[64] G. Caprino, V. Lopresto, A. Langella, C. Leone, Damage and energy absorption in GFRP laminates impacted at low-velocity: indentation model, Procedia Eng. 10 (2011) 2298–2311, http://dx.doi.org/10.1016/j.proeng.2011.04.380.

[65] M. Schwab, H.E. Pettermann, Modelling and simulation of damage and failure in large composite components subjected to impact loads, Compos. Struct. 158 (2016) 208–216, http://dx.doi.org/10.1016/j.compstruct.2016.09.041.

[66] A. Riccio, A.D. Luca, G.D. Felice, F. Caputo, Modelling the simulation of impact induced damage onset and evolution in composites, Compos. PART B 66 (2014) 340–347, http://dx.doi.org/10.1016/j.compositesb.2014.05.024.

[67] A. Riccio, F. Caputo, G. De Felice, S. Saputo, C. Toscano, V. Lopresto, A joint numerical-experimental study on impact induced intra-laminar and inter-laminar damage in laminated composites, Appl. Compos. Mater. 23 (3) (2016) 219–237, http://dx.doi.org/10.1007/s10443-015-9457-0.

[68] A. Riccio, S. Saputo, A. Sellitto, A. Raimondo, R. Ricchiuto, Numerical investigation of a stiffened panel subjected to low velocity impacts, Key Eng. Mater. 1662-9795, 665 (2015) 277–280, http://dx.doi.org/10.4028/www.scientific.net/KEM.665.277.

[69] A.F. Johnson, N. Toso-Pentecôte, S. Kilchert, Validation of damage modelling in composite fuselage structures under high velocity impact, CEAS Aeronaut. J. 4 (3) (2013) 253–264, http://dx.doi.org/10.1007/s13272-013-0071-2.

[70] R. Olsson, M.V. Donadon, B.G. Falzon, Delamination threshold load for dynamic impact on plates, Int. J. Solids Struct. 43 (10) (2006) 3124–3141, http://dx.doi.org/10.1016/j.ijsolstr.2005.05.005.

[71] D. Dugdale, Yielding of steel sheets containing slits, J. Mech. Phys. Solids 8 (2) (1960) 100–104 http://linkinghub.elsevier.com/retrieve/pii/0022509660900132 http://dx.doi.org/10.1016/0022-5096(60)90013-2 arXiv:0021-8928(59)90157-1.

[72] G.I. Barenblatt, The mathematical theory of equilibrium of crack in brittle fracture, Adv. Appl. Mech. 7 (1962) 55–129 Last accessed: 14/04/2016, arXiv:S0065-2156(08)70121-2.

[73] A. Turon, C. Dávila, P.P. Camanho, J. Costa, An engineering solution for mesh size effects in the simulation of delamination using cohesive zone models, Eng. Fract. Mech. 74 (10) (2007) 1665–1682 http://linkinghub.elsevier.com/retrieve/pii/S0013794406003808http://dx.doi.org/10.1016/j.engfracmech.2006.08.025.

[74] P.W. Harper, S.R. Hallett, Cohesive zone length in numerical simulations of composite delamination, Eng. Fract. Mech. 75 (16) (2008) 4774–4792, http://dx.doi.org/10.1016/j.engfracmech.2008.06.004.

[75] E. Panettieri, D. Fanteria, F. Danzi, A sensitivity study on cohesive elements parameters: towards their effective use to predict delaminations in low-velocity impacts on composites, Compos. Struct. 137 (2016) 130–139, http://dx.doi.org/10.1016/j.compstruct.2015.11.011.

[76] J.-L. Chaboche, Continuous damage mechanics — a tool to describe phenomena before crack initiation, Nucl. Eng. Des. 64 (1981) 233–247.

[77] A. Matzenmiller, J. Lubliner, R.L. Taylor, A constitutive model for anisotropic damage in fiber-composites, Mech. Mater. 20 (1995) 125–152.

[78] W.H. Macaulay, A note on the deflection of beams, Messenger Math. 48 (1919) 129–130.

[79] Z. Hashin, Failure criteria for unidirectional fiber composites, J. Appl. Mech. 47 (1980) 329–334.

[80] N. Hongkarnjanakul, C. Bouvet, S. Rivallant, Validation of low velocity impact modelling on different stacking sequences of CFRP laminates and influence of fibre failure, Compos. Struct. 106 (2013) 549–559, http://dx.doi.org/10.1016/j.compstruct.2013.07.008.

[81] Simulia, Abaqus Analysis User's Guide, (2015).

[82] M. Schwab, M. Todt, H.E. Pettermann, S. Biomechanics, Simulation of the Intermediate Velocity Impact Behaviour of Woven Composite Laminates Applying, 20Th int. Conf. Compos. Mater., no. July, Copenhagen, 2015, pp. 19–24.

[83] A. International, ASTM D7136 — Standard Test Method for Measuring the Damage Resistance of a Fiber-Reinforced Polymer Matrix Composite to a Drop-Weight Impact Event, (2005), http://dx.doi.org/10.1520/D7136.

[84] D.I. f. N. E.V., DIN EN 6038 — Bestimmung der Restdruckfestigkeit nach Schlagbeanspruchung, (1996).

[85] AITM 1-0010 Determination of Compression Strength After Impact, (2005).

[86] M. Abir, T. Tay, M. Ridha, H. Lee, On the relationship between failure mechanism and compression after impact (CAI) strength in composites, Compos. Struct. 182 (July) (2017) 242–250 http://linkinghub.elsevier.com/retrieve/pii/S026382231732384Xhttp://dx.doi.org/10.1016/j.compstruct.2017.09.038.

[87] C.P. Dienel, T. Qaimari, A Finite Element Study on the Influence of Delamination Shape on Residual Compressive Behavior of Single and Multiple Delaminated Composite Structures, Proc. 5th Int. Work. Aircr. Syst. Technoplogies, Shaker Verlag Aachen, Hamburg, 2015, pp. 335–344.

[88] Hexcel, HexPly M91 Product Data & User Guide, (2010) http://www.hexcel.com/Resources/DataSheets/Prepreg-Data-Sheets/M91_global.pdf.

[89] P. Maimí, P.P. Camanho, J. Mayugo, C. Dávila, A continuum damage model for composite laminates: part II — computational implementation and validation, Mech. Mater. 39 (10) (2007) 909–919 http://linkinghub.elsevier.com/retrieve/pii/S0167663607000555http://dx.doi.org/10.1016/j.mechmat.2007.03.006.

[90] J.-H. Choi, F.-K. Chang, A model for predicting damage in graphite/epoxy laminated composites resulting from low-velocity point impact, J. Compos. Mater. 26 (14) (1992) 2134–2169, http://dx.doi.org/10.1177/002199839202601408.

[91] R. Courant, K. Friedrichs, H. Lewy, On the Partial Difference Equations of Physics, Tech. Rep. New York University, New York, 1956.

[92] U.P. Breuer, Testing, Springer International Publishing, Cham, 2016, pp. 133–140, http://dx.doi.org/10.1007/978-3-319-31918-6_5 Chap. 5.

[93] S.T. Pinho, P. Robinson, L. Iannucci, Fracture toughness of the tensile and compressive fibre failure modes in laminated composites, Compos. Sci. Technol. 66 (13) (2006) 2069–2079, http://dx.doi.org/10.1016/j.compscitech.2005.12.023.

[94] A. Faggiani, B. Falzon, Predicting low-velocity impact damage on a stiffened composite panel, Compos. Part A Appl. Sci. Manuf. 41 (6) (2010) 737–749, http://dx.doi.org/10.1016/j.compositesa.2010.02.005.

[95] A. Laulusa, O. Bauchau, J.-Y. Choi, V. Tan, L. Li, Evaluation of some shear deformable shell elements, Int. J. Solids Struct. 43 (17) (2006) 5033–5054 http://linkinghub.elsevier.com/retrieve/pii/S0020768305005238http://dx.doi.org/10.1016/j.ijsolstr.2005.08.006.

[96] C.P. Dienel, Modeling the Behavior of Impact Induced Multiple Delaminations under Compressive Load, Proc. Am. 29th Tech. Conf. Compos. Mater., no. 1, American Society for Composites, San Diego, USA, 2014, , http://dx.doi.org/10.1007/s13398-014-0173-7.2 arXiv:1011.1669v3.

[97] L. De Lorenzis, G. Zavarise, Cohesive zone modeling of interfacial stresses in plated beams, Int. J. Solids Struct. 46 (24) (2009) 4181–4191, http://dx.doi.org/10.1016/j.ijsolstr.2009.08.010.

[98] M. Schwab, M. Todt, M. Wolfahrt, H. Pettermann, Failure mechanism based modelling of impact on fabric reinforced composite laminates based on shell elements, Compos. Sci. Technol. 128 (2016) 131–137 http://www.sciencedirect.com/science/article/pii/S0266353816301208http://dx.doi.org/10.1016/j.compscitech.2016.03.025.